Chemical data quantify *Deepwater Horizon* hydrocarbon flow rate and environmental distribution

T.B. Ryerson[*¶], R. Camilli[†], J.D. Kessler[‡], E.B. Kujawinski[§], C.M. Reddy[§], D.L. Valentine[+], E.L. Atlas[#], D.R. Blake[£], J.A. de Gouw[*°], S. Meinardi[£], D.D. Parrish[*], J. Peischl[*°], J.S. Seewald[§], and C. Warneke[*°]

[*]*Chemical Sciences Division, NOAA Earth System Research Laboratory, Boulder, CO 80305;* [†]*Applied Ocean Physics and Engineering Department, Woods Hole Oceanographic Institution, Woods Hole, MA 02543;* [‡]*Department of Oceanography, Texas A&M University, College Station, TX 77843;* [§]*Department of Marine Chemistry and Geochemistry, Woods Hole Oceanographic Institution, Woods Hole, MA 02543;* [+]*Department of Earth Science and Marine Science Institute, University of California, Santa Barbara 93106;* [#]*Rosenstiel School of Marine and Atmospheric Science, University of Miami, Miami, FL 33149;* [£]*Department of Chemistry, University of California, Irvine, CA 92697;* [°]*Cooperative Institute for Research in Environmental Sciences, University of Colorado, Boulder, CO 80309*

Author contributions: TR, RC, JK, EK, CR, and DV designed research and contributed equally to this work; all authors performed research and analyzed data; and TR, RC, JK, CR, and DV wrote the paper.

The authors declare no conflict of interest.

Abbreviations: DWH, Deepwater Horizon; ROV, remotely operated vehicle; GOR, gas to oil ratio; GC-FID, gas chromatography-flame ionization detection; LMRP, lower marine riser package; BTEX, benzene, toluene, ethylbenzene, and total xylenes; PAHs, polycyclic aromatic hydrocarbons; DOSS, dioctyl sodium sulfosuccinate (di-(2-ethylhexyl) sodium sulfosuccinate); FWHM, full width at half maximum; pptv, parts per trillion by volume.

[¶]corresponding author: thomas.b.ryerson@noaa.gov, tel. 303-497-7531, fax 303-497-5126

Classification:

Major Category: PHYSICAL SCIENCES

Minor Category: Environmental Sciences

\body

Abstract.

Detailed airborne, surface, and subsurface chemical measurements, primarily obtained in May and June 2010, are used to quantify initial hydrocarbon compositions along different transport pathways – in deep subsurface plumes, in the initial surface slick, and in the atmosphere – during the *Deepwater Horizon* (*DWH*) oil spill. Atmospheric measurements are consistent with a limited area of surfacing oil, with implications for leaked hydrocarbon mass transport and oil drop size distributions. The chemical data further suggest relatively little variation in leaking hydrocarbon composition over time. While readily soluble hydrocarbons made up ~25% of the leaking mixture by mass, subsurface chemical data show these compounds made up ~69% of the deep plume mass; only ~31% of deep plume mass was initially transported in the form of trapped oil droplets. Mass flows along individual transport pathways are also derived from atmospheric and subsurface chemical data. Subsurface hydrocarbon composition, dissolved oxygen, and dispersant data are used to provide a new assessment of release of hydrocarbons from the leaking well. We use the chemical measurements to estimate that (7.8±1.9) $x10^6$ kg of hydrocarbons leaked on June 10, 2010, directly accounting for roughly three-quarters of the total leaked mass on that day. The average environmental release rate of (10.1 ± 2.0) $x10^6$ kg/day derived using atmospheric and subsurface chemical data agrees within uncertainties with the official average leak rate of (10.2 ± 1.0) $x10^6$ kg/day derived using physical and optical methods.

\body

Introduction.

Knowledge of the composition, distribution, and total mass of the hydrocarbon mixture (gas plus oil) emitted following loss of the *Deepwater Horizon* (*DWH*) drilling unit is essential to plan mitigation approaches and to assess environmental impacts of the resulting spill. Estimates of *DWH* hydrocarbon flow rate were originally derived using physical and optical methods applied during the spill; values were subsequently refined and an official government estimate of oil flow rate was published (1). Analysis of airborne atmospheric chemical data provided information on hydrocarbon evaporation into the air and a lower limit to the flow rate (2); however, a more detailed description of environmental distribution has not been available. Here we present combined atmospheric, surface, and subsurface chemical data to better constrain physical transport pathways, and the resulting composition and mass flow rate of *DWH* hydrocarbon mixtures along each pathway, following subsurface release from the leaking well in early- to mid-June 2010.

Our analysis primarily focuses on the period following installation of Top Hat #4 on June 3 (3), which includes flights by a chemically-instrumented P-3 aircraft (2, 4) and ROV sampling of leaking fluid at the well (5), and ends roughly in late June at the conclusion of the R/V *Endeavor* cruise (Fig. S1). The suite of deployed subsurface, surface, and airborne measurements offers spatial, temporal, and chemical detail that is unique to this period and to this spill. We use atmospheric, surface, and subsurface measurements of hydrocarbons, dissolved oxygen, and dispersant from throughout this period, and consider additional chemical data following closure of the well, to define the

initial compositions, distributions, and mass flow rates of the hydrocarbon mixtures evolving along different pathways following release into the marine environment.

Results.

1. Composition data constrain physical transport pathways

DWH hydrocarbons were released at ~1500 m depth in a high-pressure jet, resulting in gas bubbles and liquid oil droplets with an initial number and volume distribution that is not yet well quantified (1). Size and chemical composition of the hydrocarbon bubbles and droplets evolved extremely rapidly following release from the well (6). A complex interplay of physical processes determined hydrocarbon-water plume mixing dynamics (7, 8) and affected the composition and three-dimensional distribution of the hydrocarbon mixtures within the water column, at the surface in the resulting oil slick, and in the overlying atmosphere (2).

Prediction of mass fluxes along environmental transport pathways following a deepwater blowout requires accurate understanding of time-dependent dynamical behavior and evolving chemical composition along various transport pathways, on time scales of seconds to weeks following release. Three observed features of the *DWH* spill offer key insights into marine transport pathways:

a. **Short surfacing time constrains oil droplet size.** Visual observations from response vessels suggested a ~3-hour lag time between deliberate intervention at the well and the onset of change in the fresh surface slick. This time corresponds to a mean buoyant velocity of 0.14 m/sec from 1500 m depth and is generally

consistent with the 70-minute surfacing time observed during the DeepSpill experiment following an intentional release of gas and oil from 844 m depth in the North Sea (9). Further, narrow atmospheric plumes observed under nearly orthogonal wind directions on June 8 and June 10, 2010 by the NOAA P-3 aircraft (2) indicate that the surface expression was limited to a small area laterally offset 1.0±0.5 km from the well, a finding also consistent with observations from the DeepSpill experiment (9). Acoustic Doppler current profiler data recorded at the well site (www.ndbc.noaa.gov/download_data.php?filename=42916b2010.txt.gz&dir=data/historical/adcp2/) indicate a net horizontal velocity (integrating from depths of 1200 m to the surface) of ~0.03 m/sec on June 8 and 10, 2010. Combined with the lateral offset at the surface, this would imply a mean vertical transport time of no more than ~10 hours, corresponding to a mean buoyant velocity of no less than ~0.05 m/sec. The 3-10 hour lag time indicates that droplets with ~millimeter-scale diameters transported the majority of the surfacing hydrocarbon mass (Figs. S3a and b) (10, 11). This average diameter is consistent with visual observations of droplet size distributions within the near-field plume source regions, both prior to and after shearing of the well riser pipe (5, 12), and approaches the maximum stable droplet diameter of ~10 mm (13).

b. Small surfacing area implies a narrow droplet mass distribution. Gaussian fits to data in the narrow atmospheric plume of hydrocarbons, with no detectable volatile hydrocarbon mass outside of the narrow plume (Fig. 1b) ~10 km downwind of *DWH* (2) imply that essentially all of the buoyant mass surfaced

within a ~2 km^2 area (Fig. 1a and b). This is a robust result, as the airborne instruments were sufficiently sensitive to have detected and quantified a similar mass of oil surfacing over an area of ~2000 km^2 with a plume signal-to-noise ratio of ~60 for alkanes and ~25 for aromatics (Fig. S2). However, the airborne measurements provide strong evidence that negligible mass surfaced outside of the ~2 km^2 area immediately adjacent to the spill site (Figs. 1c and d).

c. Atmospheric hydrocarbon relationships imply minimal variability in surfacing times. Within the atmospheric plume, the tight correlations and single molar enhancement ratios, defined as $\Delta[X_A]/\Delta[X_B]$ between pairs of alkanes A and B with different solubility and volatility, and aromatic-alkane pairs of different solubility (Fig. 1c and d), provide further direct evidence for a narrow distribution of surfacing times. Surfacing times appreciably shorter or longer than 3-10 hours would have resulted in lesser or greater removal of partially soluble hydrocarbons and thus variable atmospheric enhancement ratios for a given hydrocarbon pair. The tight correlation between each hydrocarbon pair (Fig. 1) provides further evidence for a narrow mass distribution of large droplets (11).

The available atmospheric observations thus argue for a single pathway transporting the majority of surfacing hydrocarbon mass directly and promptly to the surface. We conclude that the surface oil slick was fed primarily by this single pathway, with negligible mass transported to the surface via smaller droplets surfacing after longer transport times and thus at greater distances from the well (Fig. 1a).

The available subsurface observations have been described in detail elsewhere (5, 14-22). These reports conclude that the majority of subsurface mass was detected generally between 1000 and 1300 m depth in concentrated deep hydrocarbon plumes. This finding is consistent with a physical mechanism that predicts formation of horizontal intrusions, or plumes, of dissolved species and small undissolved droplets of liquid oil formed in the turbulent *DWH* jet (8). Although concentration enhancements outside of these plume depths have been reported (*e.g.*, (17, 21)) no significant *DWH* hydrocarbon mass enhancement above or below these discrete layers is evident in the subsurface chemical data to date (5, 14-22). Numerical simulations of this mechanism predict the observed depth of the deep plumes (8) and further predict additional discrete plumes at shallower depths with negligible mass compared to the deep plumes.

In the following sections we interpret the available chemical data in terms of a simplified model in which leaked *DWH* hydrocarbon mass was transported primarily along two initial pathways, either directly into the deep plume or directly to the surface; after surfacing, further evaporation into the air occurred (Fig. 1a).

2. Composition data quantify partitioning into dissolved, evaporated, and undissolved hydrocarbon mixtures

Here we compare the measured hydrocarbon compositions of atmospheric and subsurface *DWH* plume samples to the composition leaking from the Macondo well; observed differences define the extent and nature of alteration due to dissolution and evaporation over time along different transport pathways (2). The hydrocarbon composition of subsurface samples can further be altered on multi-day time scales by

differential biodegradation during transport from the well (14, 16, 17, 19, 21). To minimize this confounding effect, the analysis here considers hydrocarbon composition data from the closest and most concentrated subsurface samples, *i.e.*, those taken within 5 km of the well and characterized by very large concentration enhancements (CH_4 > 45,000 ng/µL seawater or toluene > 1,000 ng/µL seawater).

Leaking fluid composition data defines transported mixtures.

The *DWH* drilling unit was destroyed due to uncontrolled high-pressure release of natural gas and liquid oil (3). The hydrocarbon composition leaking into the Gulf of Mexico may have differed from the composition measured in the pre-spill reservoir, due to potentially abrupt reservoir composition changes associated with the blowout, phase separation, fractionation, or gas washing (23) within the flowing reservoir during the ensuing 83-day spill. A previous report (2) calculated the distribution of gas and oil compounds between the atmosphere and the water column, and a lower limit to the leaking mass flow rate, by assuming the composition of leaking fluid was unchanged from the pre-spill reservoir composition. This assumption resulted in a large uncertainty in the lower limit flow rate calculated from airborne atmospheric hydrocarbon data alone (2). This uncertainty is minimized, and partitioning and mass flow estimates improved, by use of composition data from a sample of leaking fluid taken during the spill (5).

The hydrocarbon composition of a sample taken directly within the leaking LMRP (5) is qualitatively similar (Fig. 2a) to that inferred from pre-spill analysis of reservoir fluid (2). Different values of the derived gas-to-oil ratio (GOR) result primarily from the different abundances of compounds in the gas fraction (i.e., CH_4 through

189 isomers of C_5; Fig. 2a and Fig. S4a). Additional differences are noted but have a
190 proportionally smaller effect on the conclusions presented here. Analytical uncertainties
191 of ±5%, with no additional uncertainty due to unspecified treatment of chromatographic
192 unresolved complex material (UCM) (2) in the analysis of the leaking fluid (see Fig. S2
193 in (5)), significantly improve the utility of atmospheric data to determine hydrocarbon
194 distributions between the air and the water column and to quantify hydrocarbon mass
195 flow rates, as described separately below.

196 Use of the leaking fluid composition (5) leads to a calculated distribution of *DWH*
197 hydrocarbons between air and water similar to that previously derived using the inferred
198 pre-spill composition (2). The mass fraction of each compound *X* in air is

199

200 The numerator is the slope of a linear regression to X and 2-methylheptane measured in
201 the atmosphere, and the denominator is the mass abundance of X relative to 2-
202 methylheptane in the leaking fluid (5). Here we normalize to 2-methylheptane, but the
203 results are insensitive to the choice of undissolved and volatile hydrocarbon for the
204 denominator. The present analysis utilizes atmospheric hydrocarbon data obtained from
205 ships and the P-3 aircraft between mid-May and end of June 2010, sampling a much
206 longer time period than the two days previously reported (2). The overall picture
207 developed from this larger atmospheric data set and the leaking fluid composition is
208 qualitatively similar to that reported in (2), and is shown graphically in Fig. 2b. The air-
209 water distribution of individual hydrocarbon species reported below is highly constrained

by the chemical data; uncertainties of ±10% in the calculated distributions are determined by propagation of GC-FID calibration uncertainties of ±5% (5, 24). The general similarity of the atmospheric composition, illustrated by data taken over the period of a month, suggests little change in the average composition of the surfacing *DWH* hydrocarbon mixture during this period.

Hydrocarbon mixture remaining subsurface. *DWH* hydrocarbon transport into the subsurface resulted from two separate processes operating simultaneously during the spill (8). The first process involved dissolution of hydrocarbons from large, mm-scale diameter buoyant droplets during ascent to the surface. Continued buoyant ascent physically transported the resulting droplets out of the trapped intrusion (8), leaving behind dissolved hydrocarbons in the subsurface. The dissolved hydrocarbon composition is determined from observed differences between atmospheric *DWH* plume composition measured from surface ships and aircraft (2) and the leaking composition measured directly in the well (5). Dissolved mass fractions are given by (1 – fraction of X in air) for compounds more soluble than 2-methylheptane, and are set to zero for less soluble species (filled red squares, upper panel in Fig. 2b). Multiplying these mass fractions by leaking fluid mass abundances gives the dissolved mixture composition, which accounted for ~25% of the mass of the leaking mixture. Methane (CH_4), ethane (C_2H_6), propane (C_3H_8), and isomers of butane (C_4H_{10}) accounted for 89% of the dissolved hydrocarbon mass.

The second process transporting hydrocarbons into the persistent subsurface plumes involved physical trapping of small droplets of leaking hydrocarbon fluid (8).

Trapped small droplets are expected to remain suspended following loss of dissolved hydrocarbons into the surrounding seawater (8). We focus on the deep plume data because subsurface samples (5, 14, 16-22) show little evidence for substantial hydrocarbon mass initially deposited at depths above 1000 m or below 1300 m. The relative contribution from *a*) dissolved hydrocarbon mass and *b*) suspended droplet mass in the deep plume is estimated by comparing subsurface plume chemical composition data to the composition of the unmodified leaking fluid and to its dissolved fraction, below.

The deep plume composition is identical to that of the leaking fluid for the highly soluble species, but begins to differ for less soluble species., Published subsurface data on alkanes larger than propane, and aromatics larger than toluene (14-17), were examined for samples within 5 km of the well and for which measured methane >45,000 ng/µL of seawater or toluene > 1,000 ng/µL of seawater. These concentrated near-field plume measurements (blue squares in Figs. 3a, b, and c) are normalized to the most soluble measured compound and compared to the compositions of dissolved (red circles) and leaking (black bars) mixtures defined above. In each published data set, the observed pattern of subsurface hydrocarbons relative to measured methane reported in Joye *et al.* (2010) (Fig. 3a), benzene in Camilli *et al.* (2010) (Fig. 3b), or toluene in Hazen *et al.* (2010) (Fig. 3c), respectively, approximates the composition of just the dissolved fraction of the leaking mixture. The deep persistent subsurface plumes were primarily composed of dissolved species and were relatively depleted in the more sparingly soluble species. This finding, based on subsurface chemical measurements, is qualitatively consistent with a standard oil drop size parameterization (11) in which droplet number decreases

exponentially with increasing diameter, suggesting proportionally little mass can be transported in the form of suspended droplets of liquid oil (Fig. S3b).

However, the actual drop size distributions of the DWH leaks are not known, and may not be well described by this standard parameterization. Since transport in the subsurface is highly dependent on the actual drop size distribution (8), the mass initially suspended in the deep plumes as small droplets of oil remains one of the largest uncertainties in the *DWH* hydrocarbon budget to date. Initially suspended droplets are predicted (8), were positively identified by ROV cameras (14), and are qualitatively confirmed by published subsurface enhancements of sparingly soluble polycyclic aromatic hydrocarbons (PAHs) (15, 16). These latter composition measurements, all taken very close to (within 1 km radius of) the leaking well, are not sufficient to quantify hydrocarbon mass transported in the form of suspended droplets. No direct measurements have been presented to quantify this suspended mass to date.

To begin to address this uncertainty, here we use chemical data to define the fractional contribution of sparingly soluble compounds relative to dissolved compounds for samples taken in the deep persistent plume. An approximate estimate is afforded by further analysis of published data (16) on C_{10} to C_{32} *n*-alkanes from samples taken within the concentrated deep plume at varying distances from the well (Fig. 3d). These data show a large systematic depletion (by ~85%) of heavier *n*-alkanes relative to the highly soluble aromatic compound toluene (C_7H_8), further demonstrating that proportionally little mass was transported into the deep plume in the form of suspended small droplets. Minimal biodegradation in these samples is indicated by (*n*-C_{17}/pristane) and (*n*-C_{18}/phytane) ratios (Fig. 3d) similar to those in the leaking fluid. Sparingly soluble *n*-

279 alkane mass abundances of ~15% (range 5 to 25%; Fig. 3d) in the deep plume relative to
280 the leaking fluid suggests that 31% (range 13 to 43%) of the subsurface plume mass can
281 be accounted for by transport of hydrocarbons in the form of initially suspended droplets.
282 We note this conclusion is qualitatively consistent with *DWH* simulations showing that
283 only small droplets were trapped (8), and extrapolations from standard dispersed oil
284 droplet size parameterizations (Fig. S3b) suggesting that small droplets do not transport
285 the bulk of the mass (11). However, a different drop size distribution could also be
286 consistent with these observations. More accurate size information through the full range
287 of potential drop size diameters is needed to further constrain these extrapolations.
288
289 *Volatile mixture evaporating to the atmosphere.* Undissolved volatile and semi-
290 volatile hydrocarbons evaporate on characteristic time scales of hours to days after
291 reaching the surface (2, 4, 25). The undissolved and volatile hydrocarbon mixture
292 evaporating within 2-3 hours of surfacing (2) was determined directly with uncertainties
293 of ±10% (24) using shipborne and airborne measurements of CH_4 through *n*-C_{11}. The
294 evaporated fraction of unmeasured semi-volatile hydrocarbons greater than *n*-C_{11} is
295 calculated (Fig. S5a) using the volatility distribution of the oil mixture determined from
296 the chemical composition and the net evaporation measured in the laboratory (4). The
297 sum of volatile and semi-volatile masses (Fig. 2b) shows that 14% of the surfacing
298 mixture was both sufficiently insoluble to reach the surface and sufficiently volatile to
299 evaporate from the slick within 1-2 days of surfacing. As not all the leaked mass reached
300 the surface, a smaller percent actually evaporated; this amount is quantified below.

Summing the amounts dissolved and evaporated shows that these processes together reduced the mass of hydrocarbons in the surface slick by (1 – (0.75*0.86)) = 0.36, or approximately one-third, relative to the slick mass that would have occurred in the absence of these processes. Further evaporation of less-volatile compounds likely removed little additional mass from the slick after the second day (26). The evaporating mixture chemical composition is shown graphically in Fig. 4a; *n*-heptane, *n*-octane, *n*-nonane, and methylcyclohexane were the four most abundant hydrocarbons by mass in the evaporating mixture.

The atmospheric composition data taken aboard surface vessels and the research aircraft, together with the subsurface composition data, demonstrate relatively little variation in evaporating hydrocarbon composition from late May through the end of June 2010 (Fig. 2b). The F/V *Eugenie* cruise data were taken prior to shearing the broken riser pipe on June 2 and installation of the LMRP cap on June 3. The atmospheric data taken subsequently showed no significant change following this event (Fig. 2b), suggesting little change in the composition of the surfacing hydrocarbon mixture as a result of this intervention. The absence of atmospheric CH_4 enhancements associated with any *DWH* hydrocarbons in these data (Fig. 2b) confirms earlier reports of complete CH_4 dissolution in the subsurface (2, 18, 19, 21, 22, 27), and demonstrates that no emissions of CH_4 to the atmosphere were detected through at least the first two months of the spill. These atmospheric measurements further demonstrate that leaked benzene (C_6H_6) was nearly completely removed in the water column, minimizing its impact at the surface.

Hydrocarbon mixture remaining in the surface oil slick. Leaked and surfacing hydrocarbons that neither dissolved nor evaporated within the first 1-2 days of surfacing determined the initial composition of the persistent surface oil slick. Slick chemical composition ~2 days after surfacing is shown graphically in Fig. 4b; *n*-C_{17}, *n*- C_{16}, *n*-C_{18}, and *n*-C_{15} were the four most abundant hydrocarbons by mass in the initial surface slick. Slick composition inferred from the airborne and shipborne atmospheric data is qualitatively confirmed by GC-FID analysis of oil samples taken from R/V *Endeavor* directly in the surface slick 1.5 km horizontally from the well on June 20, 2010 (Fig. S5b, lower trace).

3. Composition data constrain mass flow along different transport pathways

The combined data sets are used to estimate the mass flow rates of leaked hydrocarbons along each of the identified transport pathways (Fig. 4d) in early June 2010 that can be accounted for by the available chemical composition measurements. These are compared to the consensus government estimate of total mass flow from the well, calculated from the official volume flow rate estimate (1) in barrels of liquid oil (Fig. S1, black circles). Total hydrocarbon mass flow rate, including the gas fraction, is calculated by multiplying the government estimate of leaked oil volume flow by 132.2 kg per stock tank barrel of liquid oil and by a mass ratio of ((gas + oil)/oil) = 1.31±0.08 measured at 1 atmosphere and 15.6 °C from the WHOI sample of leaking fluid (5) (Fig. S1, red circles),

***i). DWH* hydrocarbon mass recovered to the surface ship**

345 *Discoverer Enterprise* was the only surface ship recovering hydrocarbons in early
346 June 2010 via the installed LMRP cap (Top Hat #4); liquid oil was collected after
347 separation from recovered gas, which was combusted continuously in a flare. Airborne
348 data in the atmospheric CO_2 plume downwind of the flare on June 10 verify, within error
349 limits, gas and oil recovery rates reported for *Discoverer Enterprise* (2). We use the
350 reported value of 15402 barrels of liquid oil recovered on June 10, 2010 (13), a gas-to-oil
351 ratio (GOR) of 1600 standard cubic feet per stock tank barrel consistent with the leaking
352 fluid composition (5), and estimate a ±10% uncertainty to derive a mass flow of (2.7 ±
353 0.3) $x10^6$ kg/day of hydrocarbons recovered via the cap on June 10, with the gas fraction
354 flared and the liquid fraction collected in a tanker. Flared gas and recovered oil amounts
355 are shown schematically in Fig. 4d.
356
357 ***ii).*** **Hydrocarbon evaporation to the atmosphere.**
358 The airborne data on June 10, 2010 show a steady-state atmospheric hydrocarbon
359 mass flux of (0.46±0.23) $x10^6$ kg/day (Fig. 4d), which is the sum of directly measured
360 hydrocarbon mass evaporating within ~2-3 hours of surfacing (2) plus the lesser-volatile
361 hydrocarbon mass evaporating within 1-2 days of surfacing as inferred from atmospheric
362 aerosol data (4). The uncertainty of ±50% is primarily due to uncertainties in the
363 integration of atmospheric plume hydrocarbon data. These values are indicated in Fig.
364 4d.
365
366 ***iii).*** **Hydrocarbon flow into the surface oil slick.**

An estimate of mass flow into the surface slick is obtained by summing the dissolved and evaporated masses, and subtracting this sum from the initially buoyant plume mass (after (2), from the slope of the linear fit (red line) in Fig. S4b) of (2.0±1.0) $x10^6$ kg/day. This estimate suggests that (1.0±0.5) $x10^6$ kg/day of leaked hydrocarbons were producing the surface slick in early June.

Analysis of airborne remote sensing data from the AVIRIS instrument overflights suggested a lower limit to the average daily flow into the surface slick of (0.68 to 1.30) $x10^6$ kg/day (129,000 to 246,000 barrels of detectable liquid oil remaining on the surface 25 days after the spill began) (28). This value is consistent with the estimate from P-3 *in situ* measurements, although different amounts of hydrocarbons were being recovered to the surface on these two dates. The flow rate into the slick derived from *in situ* measurements on June 10, 2010 indicated in Fig. 4b suggests a relatively small fraction, roughly 13% of the total mass escaping the cap and leaking into the subsurface, formed the persistent, visible surface slick. This likely contributed to a low bias in early oil leak rate estimates that relied upon visual observations of the surface slick (29).

***iv).* Hydrocarbon flow into the subsurface plume.**

Subsurface hydrocarbon mass is estimated using measurements of dissolved oxygen (DO) deficits in the deep hydrocarbon plumes. Kessler et al. (2011) integrated the detected far-field plume DO deficits to estimate a total of (3.5±0.5) $x10^{10}$ moles of oxygen were consumed during bacterial respiration of *DWH* hydrocarbons, using data generated on research cruises in August-October 2010 after flow from the well had ceased. They derived a similar value using the observed near-field relationship between

DO and the surfactant dioctyl sodium sulfosuccinate (DOSS) in the deep plumes (18-20). This deficit in DO was sufficient to respire all emitted *DWH* methane in the official estimate (1), plus substantial additional mass of non-methane hydrocarbons (19). A hydrocarbon mass flux into the persistent deep plume of (3.6±0.8) $x10^6$ kg/day averaged over the 83-day spill is calculated by scaling the integrated DO anomaly by the mass of the dissolved compounds (Fig. 2b), the estimated mass of suspended droplets, and by O_2 respiration stoichiometry appropriate to each hydrocarbon in this mixture (Table S1).

This calculation assumes complete biodegradation to CO_2 of dissolved hydrocarbons, of which methane (18, 19), ethane (21), propane (21), and isomers of butane (17) account for 89% of the mass (Table S1). It further assumes that by the August-September cruise dates all hydrocarbon mass was biodegraded (Table S1). The biodegraded fraction of hydrocarbons has not been directly measured, and it is likely to have been negligible for the heaviest hydrocarbons; thus, the calculation represents a lower limit to hydrocarbon mass flow into the deep plume. We note that deriving hydrocarbon mass from the observed DO anomaly is sensitive to the assumed composition and extent of biodegradation of the subsurface plume. Error limits encompassing these sensitivities are estimated by assuming a range of 5 to 25% for the heavy *n*-alkane fractions (shaded region in Fig. 3d), leading to a range of 13 to 43% calculated for the plume mass initially transported in the form of suspended oil droplets. Under these assumptions, the calculated mass flow of (3.6±0.8) $x10^6$ kg/day into the subsurface plumes was the primary flow path for leaked *DWH* hydrocarbons, as shown in Fig. 4d, and was composed primarily of dissolved species.

***v).* Composition data constrain hydrocarbon release into the environment**

A total DO-removing potential in the deep plume of (0.041 ± 0.008) moles O_2/g of hydrocarbon is calculated (Table S1) from the deep plume chemical composition, above. Dividing this into the total integrated DO anomaly of (3.5±0.5) $x10^{10}$ moles O_2 removed over the 83 days of the spill results in an average daily environmental hydrocarbon release into the water column of (10.1±2.0) $x10^6$ kg/day (Fig. 5; Table S1). This hydrocarbon mass flow rate based on the available chemical data agrees, within the uncertainties, with the official estimate of environmental release by subtracting recovered amounts from the official flow rate of (10.3±1.2) $x10^6$ kg/day of gas and oil estimated for June 10, 2010 based on physical and optical data (1).

Discussion.

Although the totals agree quantitatively, we note that the sum of chemically detected mass flows along individual transport pathways (Fig. 4d) is lower than the average environmental release rate inferred from the DO anomaly. While the simplified model shown in Fig. 1 is generally consistent with the available subsurface and atmospheric chemical data, it does not rule out additional mass transported outside of the deep plumes but not yet detected in the chemical data. A specific gravity < 1 is expected for the mixture remaining after removal of soluble species; thus, dissolution alone is not expected to cause suspended droplets to descend out of the deep plume. A potential transport pathway could instead involve gradual ascent, on hours-to-days time scales, after the initial trapping of small hydrocarbon droplets into the deep plume (8), which would distribute the corresponding hydrocarbon mass into a larger volume of the

436 subsurface as a function of rise velocity, thus droplet size. Absent measured data
437 throughout the full range of permitted drop sizes, a model study is needed to determine
438 what fraction of the total leaked mass could be represented by the size range of initially
439 trapped droplets that subsequently exited the plume on relevant time scales.

440 Analysis of the chemical data provides an independent estimate of total
441 hydrocarbon mass flow rate against which other estimates based on physical (1, 12) or
442 optical (13, 30) methods can be compared (Fig. 5). Beyond the flow rate, the chemical
443 data provide critical information on initial environmental distribution of the different
444 mixtures resulting from transport of hydrocarbons emitted from the leaking well (e.g.,
445 Fig. 4). The information provided by a cooperative subsurface, surface, and airborne
446 chemical sampling program should therefore be an integral part of a systematic response
447 to future deepwater blowouts. Strategic cooperation during a response would
448 significantly improve the ability to quantify leaking mass and environmental impacts of
449 future spills, and would further provide a means to track and quantify the effects of
450 deliberate intervention measures, subsurface dispersant application, and well and sea-
451 floor integrity after cessation of flow. With sufficient advance preparation, joint airborne
452 and subsurface chemical sampling could provide a national rapid-response capability to
453 promptly assess deepwater well leak rates, especially for those in remote and Arctic
454 regions (2).

455

456 **Materials and Methods**

457 Leaking fluid was collected into isobaric gas-tight samplers by ROV from directly
458 within the lower marine riser package (LMRP) (5). Subsequent analyses of the gas and

459 oil composition were conducted in parallel using gas chromatography with flame
460 ionization detection (GC-FID) by Geomark Research Ltd. (www.geomarkresearch.com),
461 Alpha Analytical Laboratory (www.alphalab.com), and by WHOI with similar results (5).
462 Atmospheric hydrocarbon samples were acquired by sampling air into evacuated
463 stainless-steel canisters carried aboard three surface vessels, F/V *Eugenie*, R/V *Pelican*,
464 and R/V *Thomas Jefferson*; similar canisters were used on June 08 and 10 during two
465 *DWH* survey flights of a chemically-instrumented NOAA P-3 research aircraft (2). All
466 atmospheric samples taken aboard the vessels and aircraft flights were subsequently
467 analyzed by GC-FID or GC-mass spectrometry at the University of California at Irvine
468 (24).
469

470 **Acknowledgments**

471 This research was supported by the National Science Foundation through grants to D.
472 Blake (AGS-1049952), J. Kessler (OCE-1042650 and OCE-0849246), D. Valentine
473 (OCE-1042097 and OCE-0961725), E. Kujawinski (OCE-1045811), and R. Camilli
474 (OCE-1043976), by U.S. Coast Guard contract to R. Camilli (Contract
475 HSCG3210CR0020), and by U.S. Department of Energy grant to D. Valentine (DE-
476 NT0005667). The August, September, and October research cruises were funded by
477 NOAA through a contract with Consolidated Safety Services, Incorporated. The NOAA
478 P-3 oil spill survey flights were funded in part by NOAA and in part by a U.S. Coast
479 Guard Pollution Removal Funding Authorization to NOAA. T.R. thanks C. Brock for
480 useful discussions on drop size distributions and A. Ravishankara for critical comments
481 that helped improve the manuscript.

References

1. McNutt M, *et al.* (2011) Assessment of Flow Rate Estimates for the Deepwater Horizon/Macondo Well Oil Spill. (U.S. Department of the Interior).
2. Ryerson TB, *et al.* (2011) Atmospheric emissions from the Deepwater Horizon spill constrain air-water partitioning, hydrocarbon fate, and leak rate. *Geophysical Research Letters* 38(L07803).
3. Graham B, *et al.* (2011) Deep Water: the Gulf oil disaster and the future of offshore drilling. (National Commission on the BP Deepwater Horizon Oil Spill and Offshore Drilling).
4. de Gouw JA, *et al.* (2011) Organic aerosol formation downwind from the Deepwater Horizon oil spill. *Science* 331:1295-1299.
5. Reddy CM, *et al.* (2011) Composition and fate of gas and oil released to the water column during the Deepwater Horizon oil spill. *Proceedings of the National Academy of Sciences*.
6. Zheng L, Yapa PD, & Chen FH (2003) A model for simulating deepwater oil and gas blowouts - Part I: Theory and model formulation. *Journal of Hydraulic Research* 41(4):339-351.
7. Leifer I, Luydendyk BP, Boles J, & Clark JF (2006) Natural marine seepage blowout: contribution to atmospheric methane. *Global Biogeochemical Cycles* 20.
8. Socolofsky SA, Adams EE, & Sherwood CR (2011) Formation dynamics of subsurface hydrocarbon intrusions following the Deepwater Horizon blowout. *Geophysical Research Letters* 38(L09602).
9. Johansen Ø, Rye H, & Cooper C (2003) DeepSpill - field study of a simulated oil and gas blowout in deep water. *Spill Science and Technology Bulletin* 8(5-6):433-443.
10. Chen FH & Yapa PD (2007) Estimating the oil droplet size distributions in deepwater oil spills. *Journal of Hydraulic Research* 133(2):197-207.
11. Delvigne GAL & Sweeney CE (1988) Natural dispersion of oil. *Oil & Chemical Pollution* 4:281-310.
12. Camilli R, *et al.* (2011) Acoustic measurement of the Deepwater Horizon Macondo well flow rate. *Proceedings of the National Academy of Sciences USA.*
13. Lehr W, Bristol S, & Possolo A (2010) Oil Budget Calculator Deepwater Horizon Technical Documentation.
14. Camilli R, *et al.* (2010) Tracking hydrocarbon plume transport and biodegradation at Deepwater Horizon. *Science* 330:201-204.
15. Diercks A-R, *et al.* (2010) Characterization of subsurface polycyclic aromatic hydrocarbons at the Deepwater Horizon site. *Geophysical Research Letters* 37(L20602).
16. Hazen TC, *et al.* (2010) Deep-sea oil plume enriches indigenous oil-degrading bacteria. *Science* 330:204-208.
17. Joye SB, MacDonald IR, Leifer I, & Asper V (2011) Magnitude and oxidation potential of hydrocarbon gases release from the BP oil well discharge. *Nature Geoscience* 4.

18. Kessler JD, Valentine DL, Redmond MC, & Du M (2011) Response to Comment on "A persistent oxygen anomaly reveals the fate of spilled methane in the deep Gulf of Mexico". *Science* 332.
19. Kessler JD, *et al.* (2011) A persistent oxygen anomaly reveals the fate of spilled methane in the deep Gulf of Mexico. *Science* 331:312-315.
20. Kujawinski EB, *et al.* (2011) Fate of dispersants associated with the Deepwater Horizon oil spill. *Environmental Science and Technology* 45:1298-1306.
21. Valentine DL, *et al.* (2010) Propane respiration jump-starts microbial response to a deep oil spill. *Science* 330:208-211.
22. Yvon-Lewis SA, Hu L, & Kessler J (2011) Methane flux to the atmosphere from the Deepwater Horizon oil disaster. *Geophysical Research Letters* 38(L01602).
23. Whelan J, Eglinton L, Cathles III L, Losh S, & Roberts H (2005) Surface and subsurface manifestations of gas movement through a N-S transect of the Gulf of Mexico. *Marine and Petroleum Geology* 22(4):479-497.
24. Colman JJ, *et al.* (2001) Description of the analysis of a wide range of volatile organic compounds in whole air samples collected during PEM-Tropics A and B. *Analytical Chemistry* 73:3723-3731.
25. Fingas MF (1999) The evaporation of oil spills: development and implementation of new prediction methodology. in *1999 International Oil Spill Conference*.
26. Fingas MF (1997) Studies on the evaporation of crude oil and petroleum products: I. the relationship between evaporation rate and time. *Journal of Hazardous Materials* 56:227-236.
27. Valentine DL (2010) Measure methane to quantify the oil spill. *Nature* 465:421.
28. Clark RN, *et al.* (2010) A method for quantitative mapping of thick oil spills using imaging spectroscopy. (United States Geological Survey), pp 1-54.
29. USGS (2010) Deepwater Horizon MC252 Gulf incident oil budget: government estimates - through August 01 (day 104). (USGS).
30. Crone TJ & Tolstoy M (2010) Magnitude of the 2010 Gulf of Mexico oil leak. *Science* 330:634.

Figure legends

Figure 1. a). Scale diagram of surfacing hydrocarbon plume dimensions; the atmospheric plume data are consistent with a surface source area of ~1.6 km diameter. **b).** Gaussian fits to hydrocarbon composition data, and corresponding full widths at half maximum (FWHM) from crosswind P-3 aircraft transects of the evaporating plume 10 km downwind of *DWH*; data from a single transect are shown as an example. **c).** Data

above the detection limit (>5 parts per trillion by volume (pptv)) from all *DWH* plume transects show no evidence for different populations of *n*-C_4 through *n*-C_8 alkanes relative to *n*-C_9 (different volatilities & solubilities). **d).** Data >5 pptv from all transects show no evidence for different populations of C_7 and C_8 aromatics relative to *n*-alkanes of the same carbon number (similar volatilities, different solubilities).

Figure 2. a). Pre-spill Macondo reservoir hydrocarbon mass fraction (mass of compound per mass of reservoir fluid) (2) plotted versus leaking fluid hydrocarbon mass fraction measured during the spill in mid-June (5). Each data point represents an individual hydrocarbon compound; several are labeled for illustration. Data for methane (CH_4) through *n*-undecane ($C_{11}H_{24}$) are shown, comprising 38% of the total mass of the leaking fluid. The dashed line (blue) has a slope of unity; the slope of a linear-least-squares fit (red) is, within estimated errors, not significantly different than unity. **b).** Lower panel: Atmospheric hydrocarbon mass enhancement ratios to measured 2-methylheptane (open symbols) from research vessels and aircraft reflect the undissolved and volatile components of the leaking fluid (black bars). Upper panel: Fractions in air (open symbols) are the atmospheric enhancement ratios normalized to the expected ratio to 2-methylheptane in the leaking fluid. The dissolved fraction (filled squares) is calculated from the June 10, 2010 data.

Figure 3. a). Subsurface near-field plume data (blue) from Table 2 in Joye *et al*. (2010), normalized to measured methane, compared to the composition of leaking gas and oil (black) and the composition inferred for the mixture dissolved from the promptly

surfacing mass (red). The seven most concentrated samples (CH_4 > 45,000 nM) sampled within 5 km of the well were averaged; the isobutane and *n*-butane data were transposed, and isomer-specific pentane data were apportioned according to their relative abundance in the leaking fluid. **b).** As in **a)** using subsurface plume data from Camilli *et al.* (2010) normalized to measured benzene. **c).** As in **a)** using subsurface BTEX plume data >5µg/L of seawater from Hazen *et al.* (2010) normalized to measured toluene. **d).** As in **a)** using subsurface *n*-alkane plume data >2.5 µg/L of seawater from Hazen *et al.* (2010) normalized to measured toluene. The average and range of (0.15±0.10) used to scale the DO observations are shown by the dashed line and shading, respectively.

Figure 4. a). Evaporated hydrocarbon composition after 2 days (blue bars), **b).** surface oil slick composition after 2 days (black bars), and **c).** dissolved hydrocarbon composition (red bars). The leaking hydrocarbon composition from CH_4 through *n*-C_{39} (black line) is shown in each panel for comparison. **d).** Schematic (not to scale) of hydrocarbon mass flows in the marine environment; values are calculated for June 10, 2010 in millions of kilograms per day.

Figure 5. The left-hand bar shows *DWH* hydrocarbon mass flow, in millions of kilograms for June 10, 2010, along different environmental transport pathways calculated using the chemical composition data. The middle bar shows the calculated release into the Gulf averaged over the spill duration, and the right-hand bar shows the official estimate of total hydrocarbon mass flow averaged over the spill.

Figure 1.

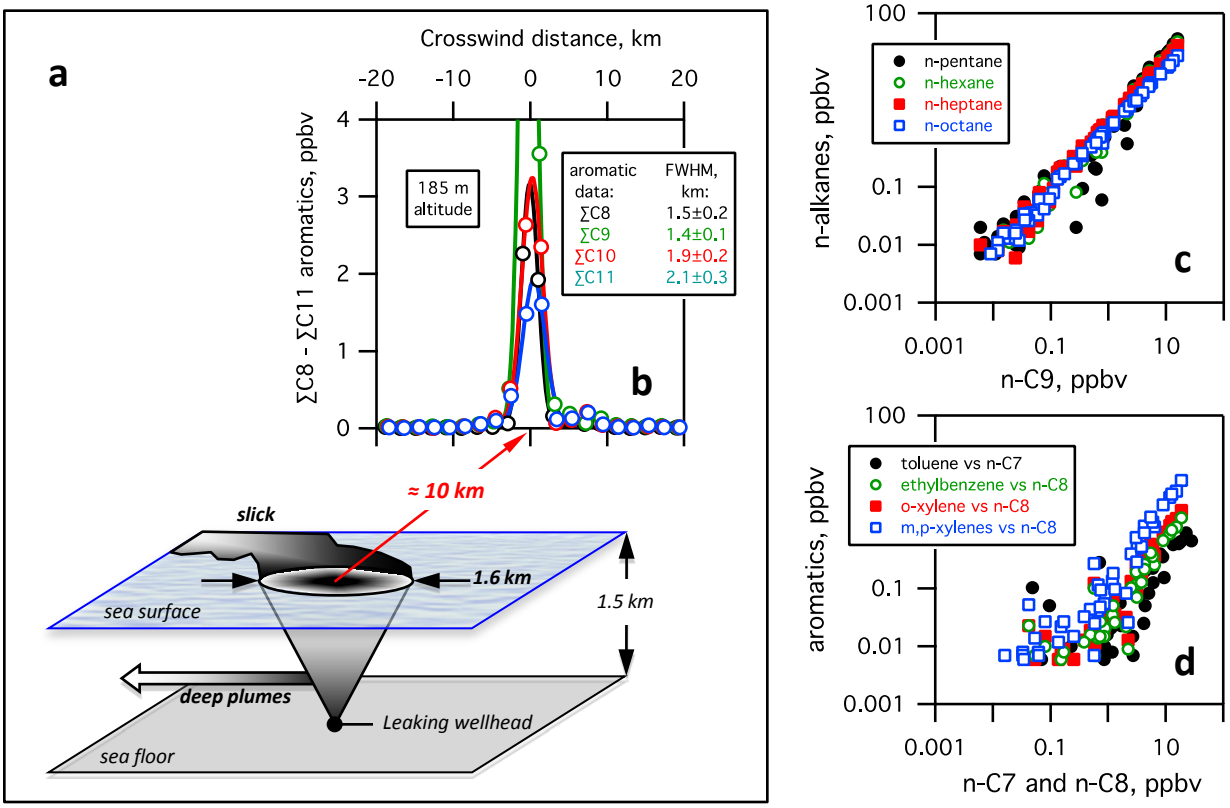
a
Crosswind distance, km
-20
-10
0
10
20
∑C8 - ∑C11 aromatics, ppbv
4
3
2
1
0
185 m altitude
aromatic data:
FWHM, km:
∑C8 1.5±0.2
∑C9 1.4±0.1
∑C10 1.9±0.2
∑C11 2.1±0.3
b
≈ 10 km
slick
1.6 km
1.5 km
sea surface
deep plumes
Leaking wellhead
sea floor
n-alkanes, ppbv
100
0.1
0.01
0.001
n-pentane
n-hexane
n-heptane
n-octane
c
0.001
0.1
10
n-C9, ppbv
aromatics, ppbv
toluene vs n-C7
ethylbenzene vs n-C8
o-xylene vs n-C8
m,p-xylenes vs n-C8
d
n-C7 and n-C8, ppbv

Figure 2.

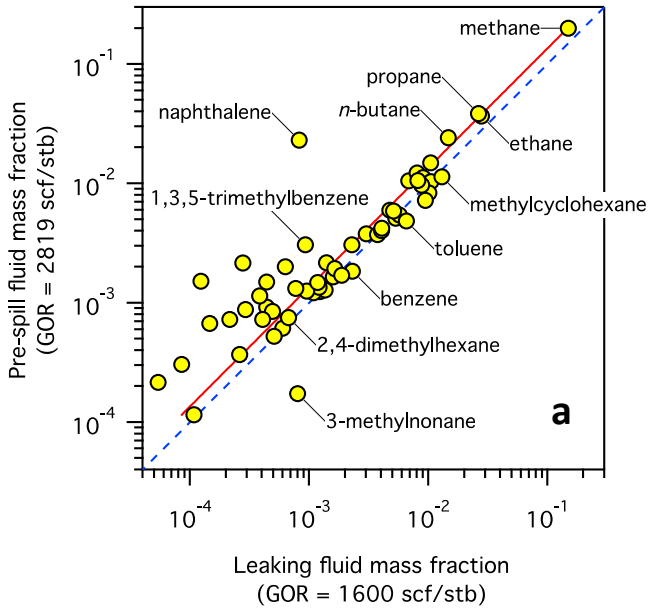
methane
propane
n-butane
ethane
naphthalene
1,3,5-trimethylbenzene
methylcyclohexane
toluene
benzene
2,4-dimethylhexane
3-methylnonane
a
Pre-spill fluid mass fraction
(GOR = 2819 scf/stb)
Leaking fluid mass fraction
(GOR = 1600 scf/stb)

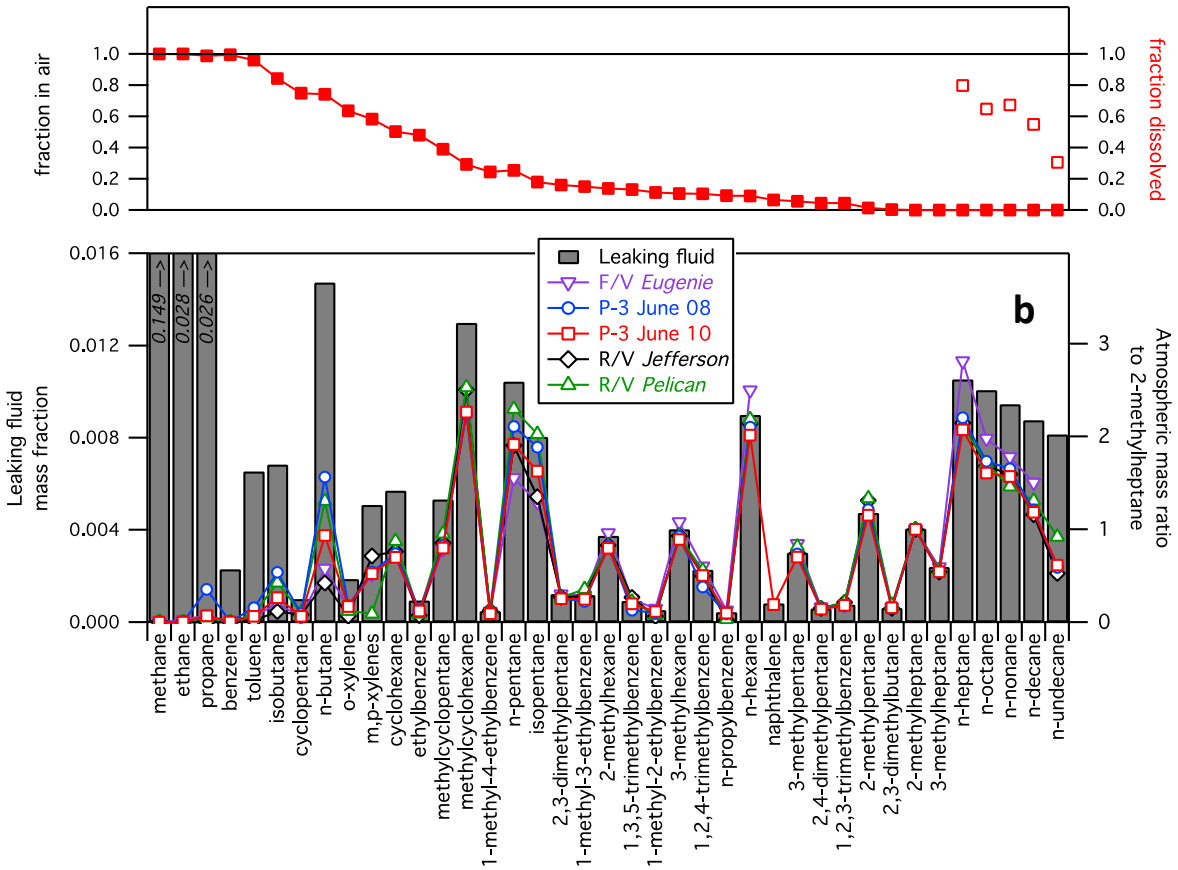
fraction in air
fraction dissolved
Leaking fluid
F/V Eugenie
P-3 June 08
P-3 June 10
R/V Jefferson
R/V Pelican
b
0.149 —>
0.028 —>
0.026 —>
Leaking fluid
mass fraction
Atmospheric mass ratio
to 2-methylheptane
methane
ethane
propane
benzene
toluene
isobutane
cyclopentane
n-butane
o-xylene
m,p-xylenes
cyclohexane
ethylbenzene
methylcyclopentane
methylcyclohexane
1-methyl-4-ethylbenzene
n-pentane
isopentane
2,3-dimethylpentane
1-methyl-3-ethylbenzene
2-methylhexane
1,3,5-trimethylbenzene
1-methyl-2-ethylbenzene
3-methylhexane
1,2,4-trimethylbenzene
n-propylbenzene
n-hexane
naphthalene
3-methylpentane
2,4-dimethylpentane
1,2,3-trimethylbenzene
2-methylpentane
2,3-dimethylbutane
2-methylheptane
3-methylheptane
n-heptane
n-octane
n-nonane
n-decane
n-undecane

Figure 3.

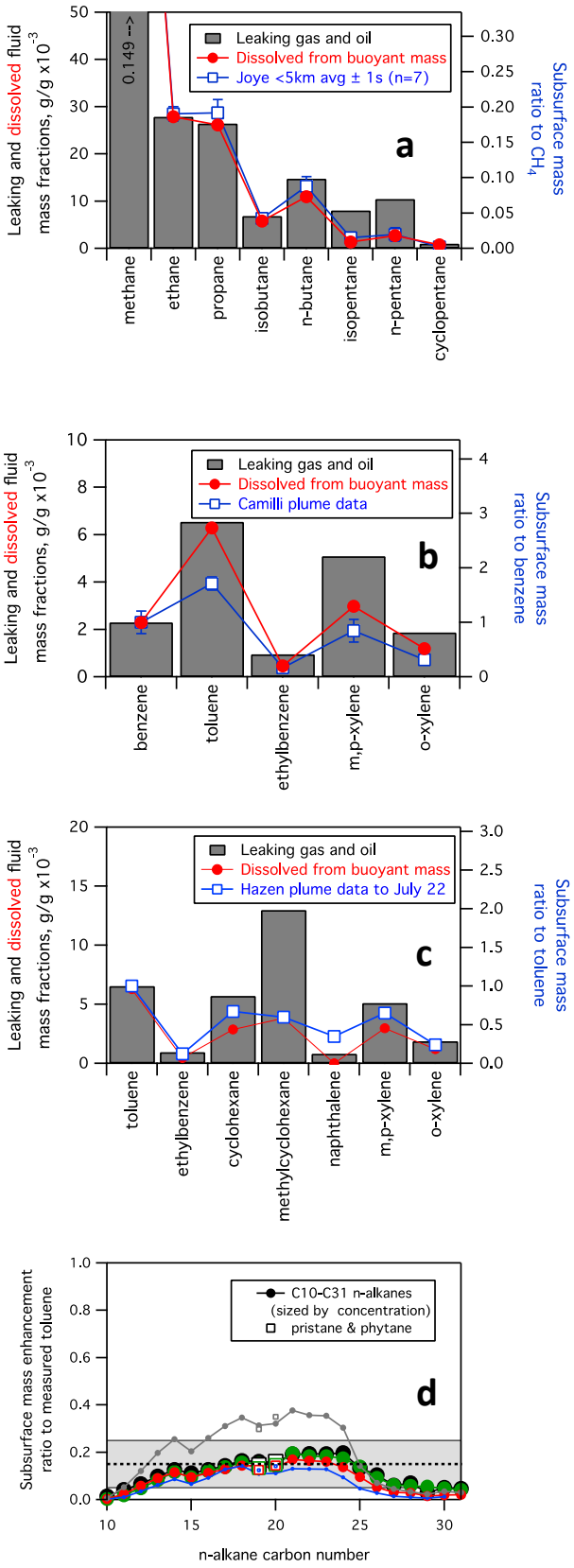
Leaking and dissolved fluid mass fractions, g/g x10-3
Subsurface mass ratio to CH4
0.149 -->
Leaking gas and oil
Dissolved from buoyant mass
Joye <5km avg ± 1s (n=7)
a
methane
ethane
propane
isobutane
n-butane
isopentane
n-pentane
cyclopentane
Leaking and dissolved fluid mass fractions, g/g x10-3
Subsurface mass ratio to benzene
Leaking gas and oil
Dissolved from buoyant mass
Camilli plume data
b
benzene
toluene
ethylbenzene
m,p-xylene
o-xylene
Leaking and dissolved fluid mass fractions, g/g x10-3
Subsurface mass ratio to toluene
Leaking gas and oil
Dissolved from buoyant mass
Hazen plume data to July 22
c
toluene
ethylbenzene
cyclohexane
methylcyclohexane
naphthalene
m,p-xylene
o-xylene
Subsurface mass enhancement ratio to measured toluene
C10-C31 n-alkanes
(sized by concentration)
pristane & phytane
d
n-alkane carbon number

Figure 4.

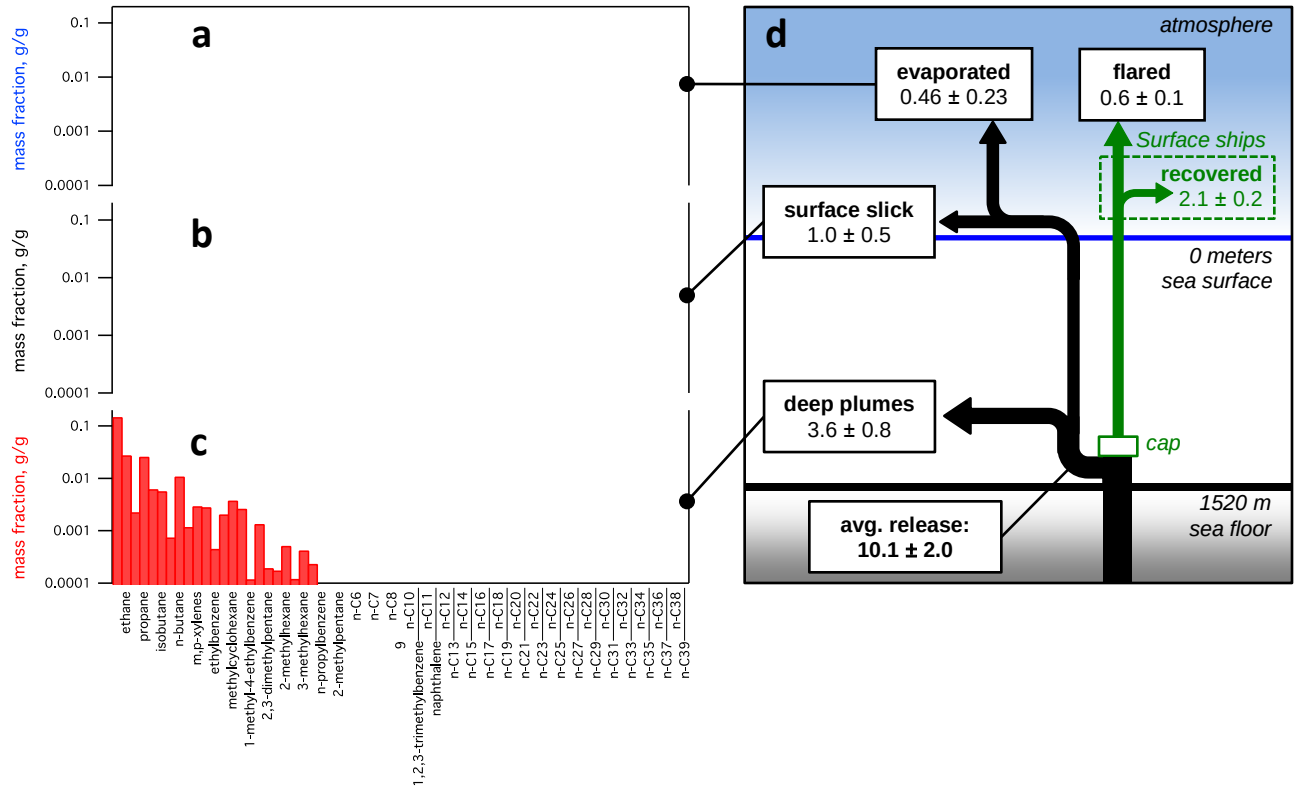
a
b
c
d
mass fraction, g/g
0.1
0.01
0.001
0.0001
ethane
propane
isobutane
n-butane
m,p-xylenes
ethylbenzene
methylcyclohexane
1-methyl-4-ethylbenzene
2,3-dimethylpentane
2-methylhexane
3-methylhexane
n-propylbenzene
2-methylpentane
n-C6
n-C7
n-C8
9
n-C10
1,2,3-trimethylbenzene
n-C11
naphthalene
n-C12
n-C13
n-C14
n-C15
n-C16
n-C17
n-C18
n-C19
n-C20
n-C21
n-C22
n-C23
n-C24
n-C25
n-C26
n-C27
n-C28
n-C29
n-C30
n-C31
n-C32
n-C33
n-C34
n-C35
n-C36
n-C37
n-C38
n-C39
atmosphere
evaporated
0.46 ± 0.23
flared
0.6 ± 0.1
Surface ships
recovered
2.1 ± 0.2
surface slick
1.0 ± 0.5
0 meters
sea surface
deep plumes
3.6 ± 0.8
cap
avg. release:
10.1 ± 2.0
1520 m
sea floor

Figure 5.

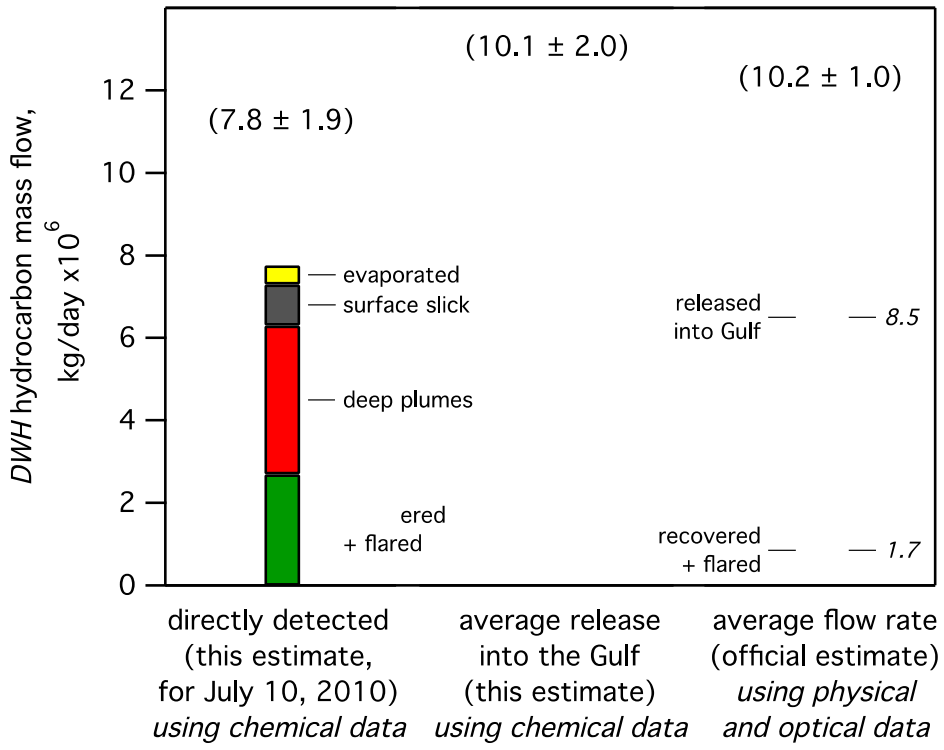
(10.1 ± 2.0)
(10.2 ± 1.0)
(7.8 ± 1.9)
12
10
8
6
4
2
0
DWH hydrocarbon mass flow, kg/day x10^6
evaporated
surface slick
deep plumes
ered
+ flared
released into Gulf
8.5
recovered + flared
1.7
directly detected (this estimate, for July 10, 2010) using chemical data
average release into the Gulf (this estimate) using chemical data
average flow rate (official estimate) using physical and optical data

Supplemental figures

SI Figure captions.

Fig. S1. Lower panel: Time series showing official estimate of total Macondo well flow rate of oil (black circles) and oil plus gas (red circles); red shading denotes 10% uncertainties stated for these estimates. Rates of oil recovery (black line) and oil plus gas recovery (red line) to surface ships are also shown. Upper panel: dates of ship cruises and aircraft flights used in this report. Dates for ship cruises following closure of the well are not shown.

Fig. S2. A Gaussian fit to the evaporating plume VOC signal detected by the P-3 aircraft at 10 km downwind (black line, with peak values offscale at 22 ppbv) was used to parameterize atmospheric plume simulations of a series of successively larger source areas (colored lines). Simulated source areas were assumed to be circular and homogeneous; other source distributions would give rise to larger atmospheric enhancements. The simulations show the P-3 would have detected an equal VOC mass evaporating over a 1000-fold larger area with a plume signal-to-noise of approximately 60 (red line), based on instrument sensitivities and the measured background alkane and aromatic concentrations of 10±10 pptv in the upwind Gulf marine boundary layer.

Fig. S3. a). Simulated oil drop rise times as a function of drop diameter; data (blue circles) are from the Oil Budget Calculator Appendix 7, Table 1 (1). Average diameters of droplets (black squares) for the range of surfacing times derived in the text are calculated by extrapolating from a fitted line to the OBC data. **b).** Oil drop size

distribution (red dashed line) extrapolated from a fit to data (blue circles) from Delvigne and Sweeney (1988) Figure 9, and the corresponding mass distribution (black).

Fig. S4. a). Lower panel: Comparison of leaking fluid mass fraction (black bars) (2) and pre-spill reservoir fluid mass fraction (red squares) (3). Upper panel: Ratio of pre-spill mass fraction to leaking fluid mass fraction; axis range shows a factor of ±2. **b).** Atmospheric mass fluxes of hydrocarbons measured on June 10, 2010 are shown for soluble (blue), insoluble and volatile (red) and less volatile (black) compounds as a function of the leaking fluid mass fraction. Benzene, ethane, and methane data are off scale due to negligible or zero atmospheric flux.

Fig. S5. a). Fraction of *n*-alkanes remaining in the surface oil slick predicted from the volatility distribution of the oil mixture. **b).** GC-FID traces (courtesy of C. Carmichael, WHOI) of the liquid oil fraction of the leaking fluid (2) (upper trace) and of a fresh oil sample collected 1.4 km from *Enterprise* in the surface oil slick (lower trace).

1. Lehr W, Bristol S, & Possolo A (2010) Oil Budget Calculator Deepwater Horizon Technical Documentation.
2. Reddy CM, *et al.* (2011) Composition and fate of gas and oil released to the water column during the Deepwater Horizon oil spill. *Proceedings of the National Academy of Sciences (submitted to DWH special issue).*
3. Ryerson TB, *et al.* (2011) Atmospheric emissions from the Deepwater Horizon spill constrain air-water partitioning, hydrocarbon fate, and leak rate. *Geophysical Research Letters* 38(L07803).

Figure S1.

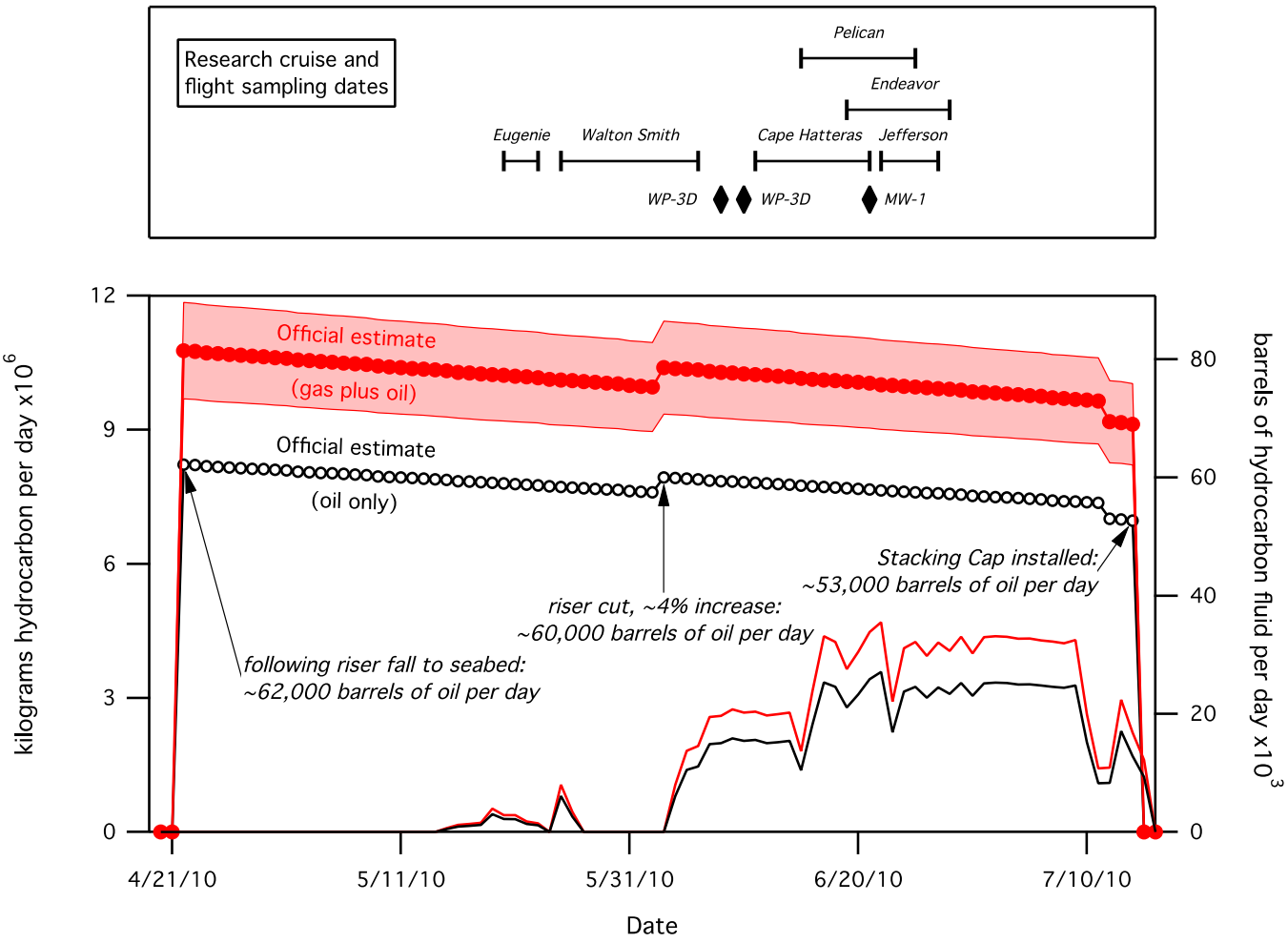
Research cruise and flight sampling dates
Pelican
Endeavor
Eugenie
Walton Smith
Cape Hatteras
Jefferson
WP-3D
WP-3D
MW-1
Official estimate
(gas plus oil)
Official estimate
(oil only)
following riser fall to seabed:
~62,000 barrels of oil per day
riser cut, ~4% increase:
~60,000 barrels of oil per day
Stacking Cap installed:
~53,000 barrels of oil per day
kilograms hydrocarbon per day x10^6
barrels of hydrocarbon fluid per day x10^3
0
3
6
9
12
0
20
40
60
80
4/21/10
5/11/10
5/31/10
6/20/10
7/10/10
Date

Figure S2.

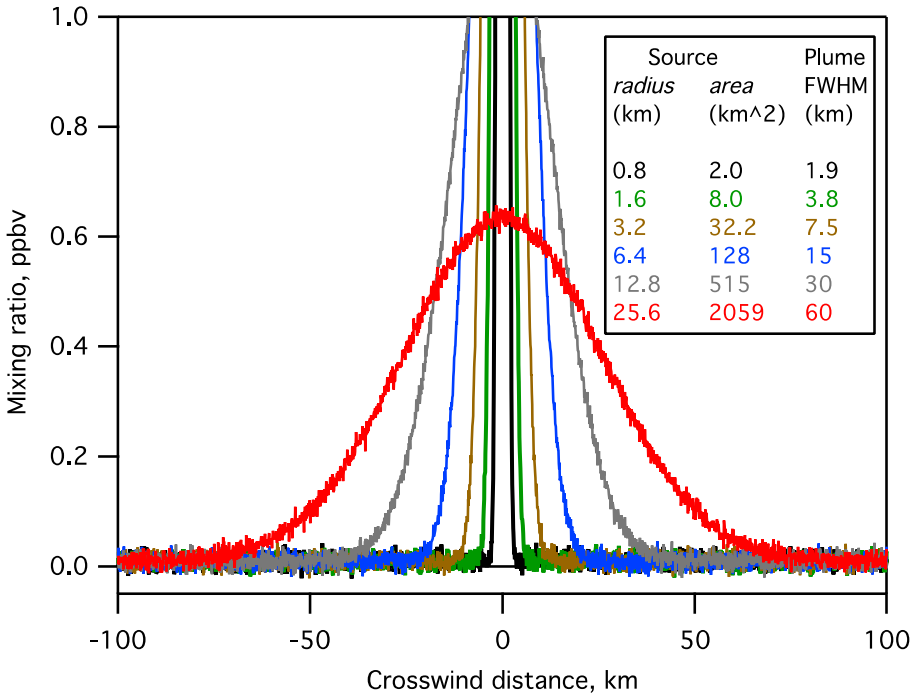
Source
radius
(km)
area
(km^2)
Plume
FWHM
(km)
0.8 2.0 1.9
1.6 8.0 3.8
3.2 32.2 7.5
6.4 128 15
12.8 515 30
25.6 2059 60
Mixing ratio, ppbv
1.0
0.8
0.6
0.4
0.2
0.0
-100
-50
0
50
100
Crosswind distance, km

Figure S3.

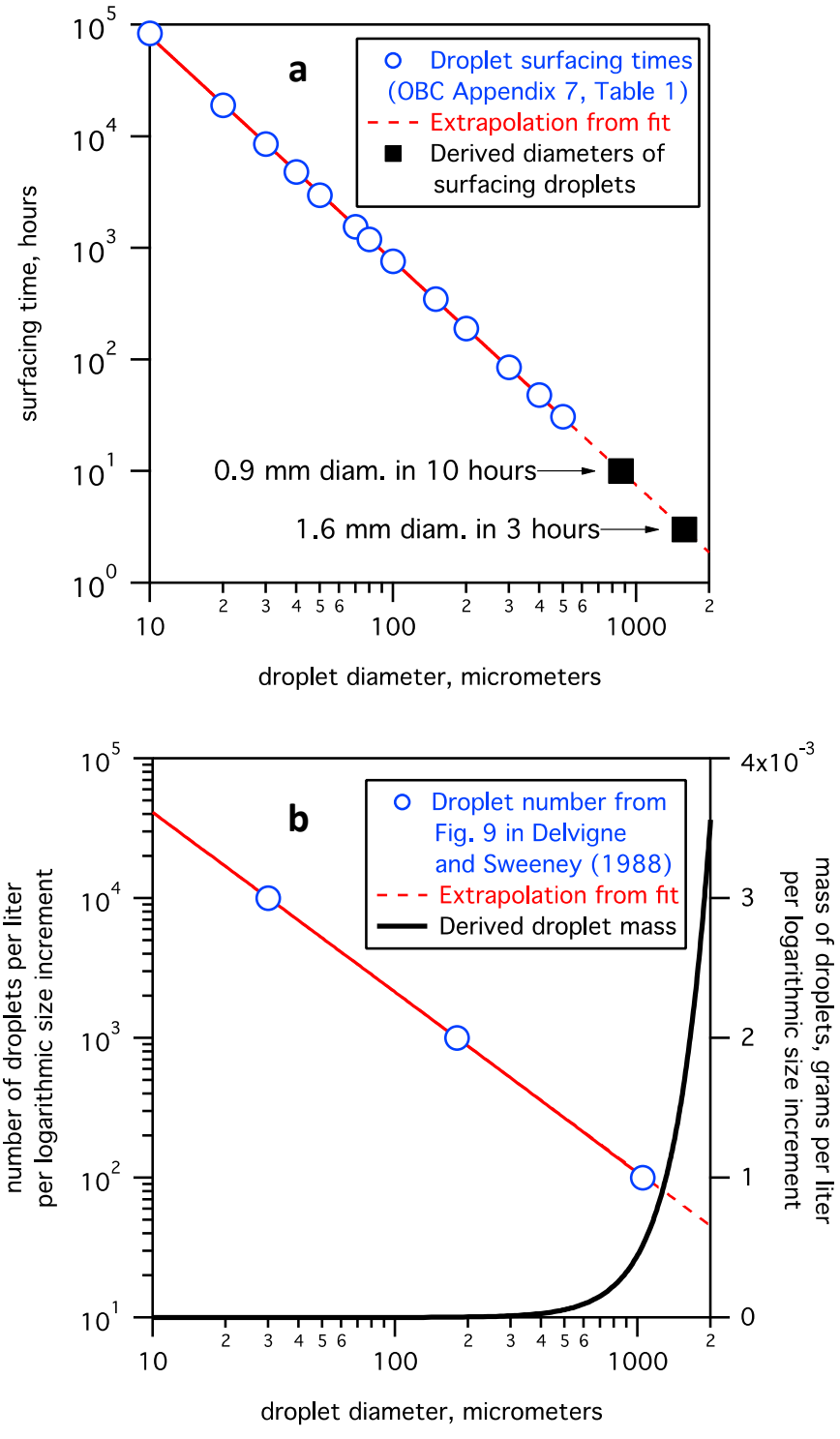
a
Droplet surfacing times
(OBC Appendix 7, Table 1)
Extrapolation from fit
Derived diameters of
surfacing droplets
0.9 mm diam. in 10 hours
1.6 mm diam. in 3 hours
surfacing time, hours
droplet diameter, micrometers
b
Droplet number from
Fig. 9 in Delvigne
and Sweeney (1988)
Extrapolation from fit
Derived droplet mass
number of droplets per liter
per logarithmic size increment
mass of droplets, grams per liter
per logarithmic size increment
droplet diameter, micrometers

Figure S4.

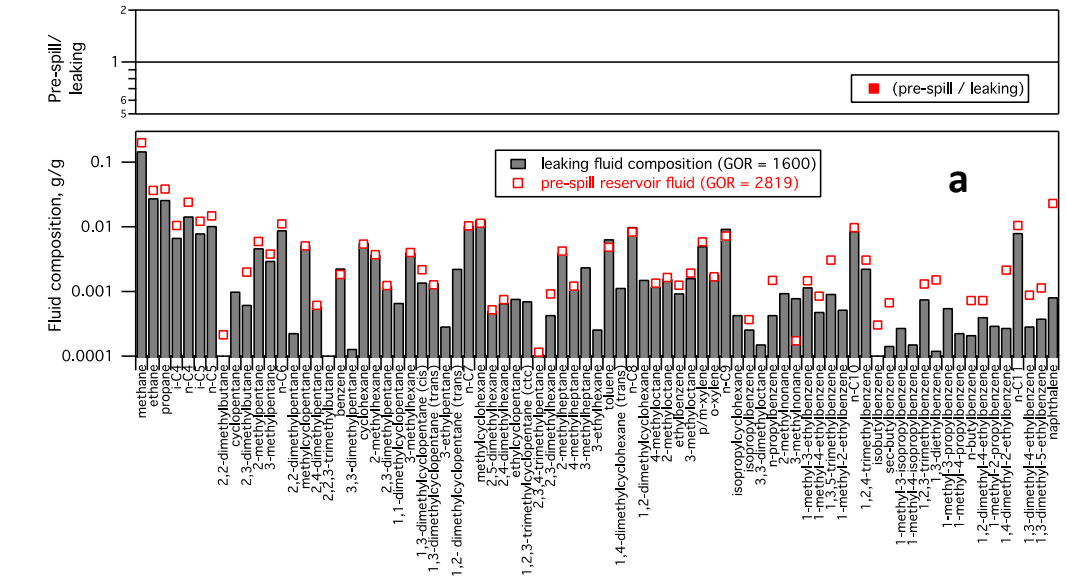
Pre-spill/ leaking
(pre-spill / leaking)
Fluid composition, g/g
leaking fluid composition (GOR = 1600)
pre-spill reservoir fluid (GOR = 2819)
a

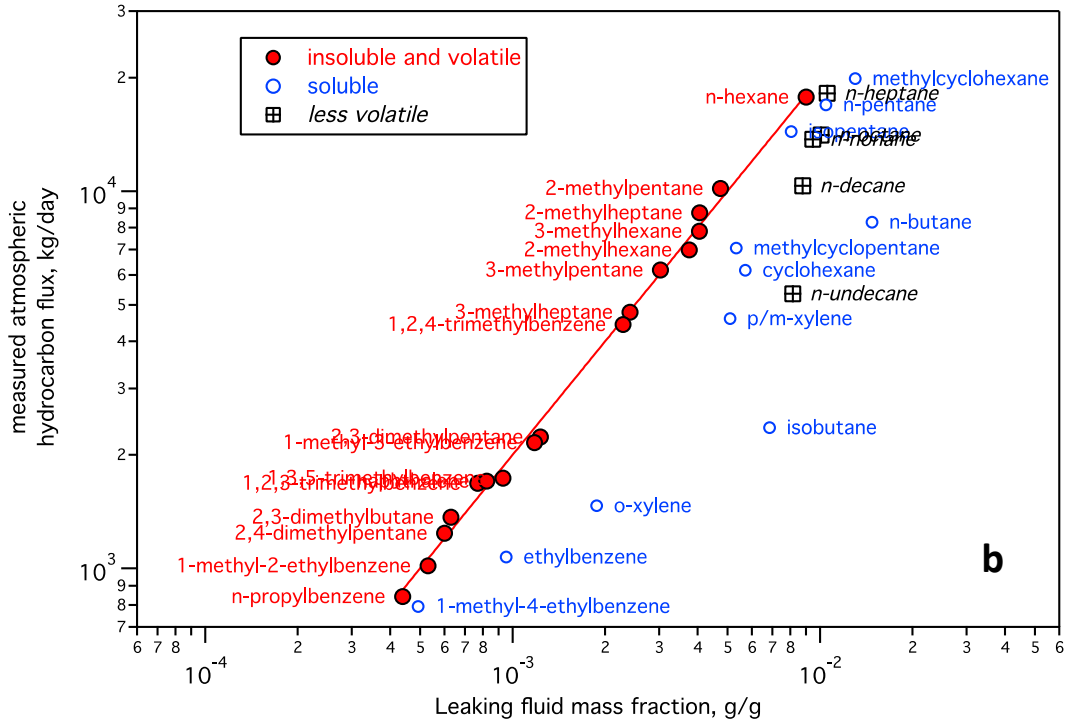
insoluble and volatile
soluble
less volatile
measured atmospheric hydrocarbon flux, kg/day
Leaking fluid mass fraction, g/g
n-hexane
2-methylpentane
2-methylheptane
3-methylhexane
2-methylhexane
3-methylpentane
3-methylheptane
1,2,4-trimethylbenzene
2,3-dimethylpentane
1-methyl-3-ethylbenzene
2,3-dimethylbutane
2,4-dimethylpentane
1-methyl-2-ethylbenzene
n-propylbenzene
methylcyclohexane
n-heptane
n-pentane
n-nonane
n-decane
n-butane
methylcyclopentane
cyclohexane
n-undecane
p/m-xylene
isobutane
o-xylene
ethylbenzene
1-methyl-4-ethylbenzene
b

Figure S5.

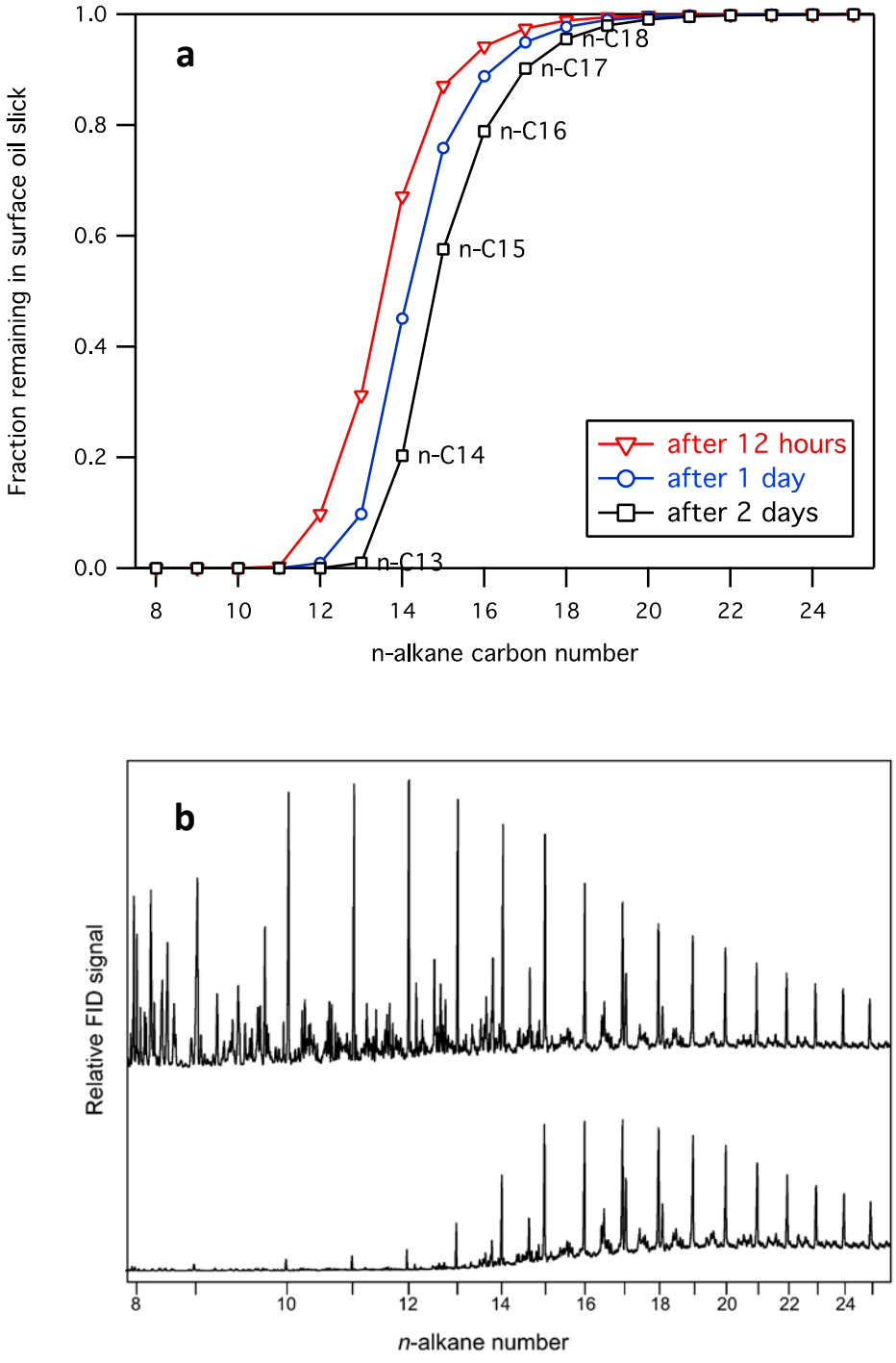
a
Fraction remaining in surface oil slick
1.0
0.8
0.6
0.4
0.2
0.0
n-C18
n-C17
n-C16
n-C15
n-C14
n-C13
after 12 hours
after 1 day
after 2 days
8
10
12
14
16
18
20
22
24
n-alkane carbon number
b
Relative FID signal
8
10
12
14
16
18
20
22
24
n-alkane number

Compound	Molec. weight (g/mol)	Mass fraction in leaking fluid (g/g_{Total})	Fraction dissolved[a]	Stoichio–metric Ratio O_2:HC[b]	DO removing potential of soluble hydrocarbons (mol O_2/g_{Total})	DO removing potential of insoluble hydrocarbons (mol O_2/g_{Total})[c]	Mass of dissolved HCs - Low (g)[d]	Mass of dissolved HCs - High (g)[e]	Mass of insoluble HCs - Low (g)[f]	Mass of insoluble HCs - High (g)[g]
	MW_i	M_i	F_i	S_i	$(F_i*M_i*S_i)/MW_i$	$((1-F_i)*M_i*S_i)*0.15*0.961)/(MW_i*F_x)$				
methane	16.042	0.14957	1	2.0	1.865E-02	0	1.31E+06	1.70E+06	0.00E+00	0.00E+00
ethane	30.069	0.02787	1	3.5	3.245E-03	0	2.44E+05	3.17E+05	0.00E+00	0.00E+00
propane	44.096	0.02642	0.9893	5.0	2.964E-03	1.496E-05	2.29E+05	2.97E+05	1.16E+03	1.50E+03
benzene	78.112	0.00230	0.9952	7.5	2.197E-04	4.987E-07	2.00E+04	2.60E+04	4.55E+01	5.91E+01
toluene	92.138	0.00654	0.9610	9.0	6.141E-04	1.167E-05	5.50E+04	7.15E+04	1.05E+03	1.36E+03
i-C_4	58.122	0.00684	0.8431	6.5	6.453E-04	5.619E-05	5.05E+04	6.57E+04	4.40E+03	5.72E+03
n-C_4	58.122	0.01474	0.7423	6.5	1.224E-03	1.987E-04	9.58E+04	1.25E+05	1.56E+04	2.02E+04
cyclopentane	70.133	0.00101	0.7501	7.5	8.078E-05	1.260E-05	6.61E+03	8.60E+03	1.03E+03	1.34E+03
o-xylene	106.165	0.00188	0.6360	10.5	1.180E-04	3.160E-05	1.04E+04	1.36E+04	2.80E+03	3.64E+03
p/m-xylene	106.165	0.00510	0.5840	10.5	2.944E-04	9.812E-05	2.61E+04	3.39E+04	8.68E+03	1.13E+04
cyclohexane	84.159	0.00570	0.5025	9.0	3.066E-04	1.420E-04	2.51E+04	3.26E+04	1.16E+04	1.51E+04
ethylbenzene	106.165	0.00095	0.4814	10.5	4.539E-05	2.288E-05	4.02E+03	5.22E+03	2.02E+03	2.63E+03
methylcyclopentane	84.159	0.00533	0.3904	9.0	2.225E-04	1.625E-04	1.82E+04	2.37E+04	1.33E+04	1.73E+04
methylcyclohexane	98.186	0.01299	0.2935	10.5	4.078E-04	4.593E-04	3.34E+04	4.34E+04	3.76E+04	4.89E+04
1-methyl-4-ethylbenzene	120.192	0.00049	0.2448	12.0	1.203E-05	1.736E-05	1.05E+03	1.37E+03	1.52E+03	1.98E+03
i-C_5	72.149	0.00805	0.2557	8.0	2.282E-04	3.108E-04	1.80E+04	2.34E+04	2.45E+04	3.19E+04
n-C_5	72.149	0.01045	0.1697	8.0	1.966E-04	4.500E-04	1.55E+04	2.02E+04	3.55E+04	4.62E+04
2,3-dimethylpentane	100.202	0.00123	0.1605	11.0	2.168E-05	5.304E-05	1.73E+03	2.25E+03	4.23E+03	5.50E+03
1-methyl-3-ethylbenzene	120.192	0.00118	0.1502	12.0	1.764E-05	4.670E-05	1.55E+03	2.01E+03	4.09E+03	5.32E+03
2-methylhexane	100.202	0.00375	0.1393	11.0	5.737E-05	1.659E-04	4.57E+03	5.95E+03	1.32E+04	1.72E+04
1,3,5-trimethylbenzene	120.192	0.00093	0.1321	12.0	1.227E-05	3.772E-05	1.08E+03	1.40E+03	3.31E+03	4.30E+03
3-methylhexane	100.202	0.00404	0.1055	11.0	4.683E-05	1.858E-04	3.73E+03	4.85E+03	1.48E+04	1.93E+04
1,2,4-trimethylbenzene	120.192	0.00228	0.1039	12.0	2.370E-05	9.558E-05	2.08E+03	2.70E+03	8.38E+03	1.09E+04
n-propylbenzene	120.192	0.00044	0.0932	12.0	4.077E-06	1.856E-05	3.57E+02	4.65E+02	1.63E+03	2.12E+03
1,2,3-trimethylbenzene	120.192	0.00077	0	12.0	0	3.591E-05	0.00E+00	0.00E+00	3.15E+03	4.09E+03
2,2-dimethylbutane	86.175	0.00005	0	9.5	0	2.776E-06	0.00E+00	0.00E+00	2.20E+02	2.87E+02
2,3-dimethylbutane	86.175	0.00063	0	9.5	0	3.252E-05	0.00E+00	0.00E+00	2.58E+03	3.36E+03

2-methylpentane	86.175	0.00474	0	9.5	0	2.447E-04	0.00E+00	0.00E+00	1.94E+04	2.53E+04
3-methylpentane	86.175	0.00302	0	9.5	0	1.558E-04	0.00E+00	0.00E+00	1.24E+04	1.61E+04
n-C_6	86.175	0.00900	0	9.5	0	4.640E-04	0.00E+00	0.00E+00	3.68E+04	4.79E+04
2,2-dimethylpentane	100.202	0.00023	0	11.0	0	1.185E-05	0.00E+00	0.00E+00	9.45E+02	1.23E+03
2,4-dimethylpentane	100.202	0.00060	0	11.0	0	3.080E-05	0.00E+00	0.00E+00	2.46E+03	3.19E+03
2,2,3-trimethylbutane	100.202	0.00005	0	11.0	0	2.369E-06	0.00E+00	0.00E+00	1.89E+02	2.46E+02
3,3-dimethylpentane	100.202	0.00013	0	11.0	0	6.713E-06	0.00E+00	0.00E+00	5.35E+02	6.96E+02
1,1-dimethylcyclopentane	98.186	0.00068	0	10.5	0	3.385E-05	0.00E+00	0.00E+00	2.77E+03	3.60E+03
1,3-dimethylcyclopentane (*cis*)	98.186	0.00140	0	10.5	0	7.001E-05	0.00E+00	0.00E+00	5.73E+03	7.45E+03
1,3-dimethylcyclopentane (*trans)*	98.186	0.00136	0	10.5	0	6.809E-05	0.00E+00	0.00E+00	5.57E+03	7.24E+03
3-ethylpentane	100.202	0.00029	0	11.0	0	1.501E-05	0.00E+00	0.00E+00	1.20E+03	1.56E+03
1,2-dimethylcyclopentane (*trans*)	98.186	0.00228	0	10.5	0	1.139E-04	0.00E+00	0.00E+00	9.32E+03	1.21E+04
n-C_7	100.202	0.01053	0	11.0	0	5.410E-04	0.00E+00	0.00E+00	4.31E+04	5.61E+04
2,5-dimethylhexane	114.229	0.00051	0	12.5	0	2.598E-05	0.00E+00	0.00E+00	2.08E+03	2.70E+03
2,4-dimethylhexane	114.229	0.00067	0	12.5	0	3.425E-05	0.00E+00	0.00E+00	2.74E+03	3.56E+03
ethylcyclopentane	98.186	0.00078	0	10.5	0	3.885E-05	0.00E+00	0.00E+00	3.18E+03	4.13E+03
1,2,3-trimethylcyclopentane (ctc)	112.213	0.00072	0	12.0	0	3.577E-05	0.00E+00	0.00E+00	2.93E+03	3.81E+03
2,3,4-trimethylpentane	114.229	0.00011	0	12.5	0	5.511E-06	0.00E+00	0.00E+00	4.41E+02	5.73E+02
2,3-dimethylhexane	114.229	0.00044	0	12.5	0	2.244E-05	0.00E+00	0.00E+00	1.79E+03	2.33E+03
2-methylheptane	114.229	0.00406	0	12.5	0	2.078E-04	0.00E+00	0.00E+00	1.66E+04	2.16E+04
4-methylheptane	114.229	0.00109	0	12.5	0	5.590E-05	0.00E+00	0.00E+00	4.47E+03	5.81E+03
3-methylheptane	114.229	0.00241	0	12.5	0	1.232E-04	0.00E+00	0.00E+00	9.86E+03	1.28E+04
3-ethylhexane	114.229	0.00026	0	12.5	0	1.338E-05	0.00E+00	0.00E+00	1.07E+03	1.39E+03
1,4-dimethylcyclohexane (*trans*)	112.213	0.00115	0	12.0	0	5.770E-05	0.00E+00	0.00E+00	4.72E+03	6.14E+03
n-C_8	114.229	0.01007	0	12.5	0	5.157E-04	0.00E+00	0.00E+00	4.12E+04	5.36E+04
1,2-dimethylcyclohexane	112.213	0.00153	0	12.0	0	7.655E-05	0.00E+00	0.00E+00	6.27E+03	8.15E+03
4-methyloctane	128.255	0.00121	0	14.0	0	6.165E-05	0.00E+00	0.00E+00	4.94E+03	6.43E+03
2-methyloctane	128.255	0.00159	0	14.0	0	8.128E-05	0.00E+00	0.00E+00	6.52E+03	8.47E+03
3-methyloctane	128.255	0.00164	0	14.0	0	8.364E-05	0.00E+00	0.00E+00	6.71E+03	8.72E+03
n-C_9	128.255	0.00946	0	14.0	0	4.830E-04	0.00E+00	0.00E+00	3.87E+04	5.03E+04

isopropylcyclohexane	126.239	0.00044	0	13.5	0	2.193E-05	0.00E+00	0.00E+00	1.79E+03	2.33E+03
isopropylbenzene	120.192	0.00026	0	12.0	0	1.221E-05	0.00E+00	0.00E+00	1.07E+03	1.39E+03
3,3-dimethyloctane	142.282	0.00015	0	15.5	0	7.837E-06	0.00E+00	0.00E+00	6.30E+02	8.19E+02
2-methylnonane	142.282	0.00096	0	15.5	0	4.898E-05	0.00E+00	0.00E+00	3.94E+03	5.12E+03
3-methylnonane	142.282	0.00080	0	15.5	0	4.075E-05	0.00E+00	0.00E+00	3.27E+03	4.26E+03
1-methyl-2-ethylbenzene	120.192	0.00053	0	12.0	0	2.478E-05	0.00E+00	0.00E+00	2.17E+03	2.82E+03
n-C_{10}	142.282	0.00876	0	15.5	0	4.467E-04	0.00E+00	0.00E+00	3.59E+04	4.67E+04
isobutylbenzene	134.218	0.00008	0	13.5	0	3.980E-06	0.00E+00	0.00E+00	3.46E+02	4.50E+02
sec-butylbenzene	134.218	0.00015	0	13.5	0	6.874E-06	0.00E+00	0.00E+00	5.98E+02	7.78E+02
1-methyl-3-isopropylbenzene	134.218	0.00028	0	13.5	0	1.303E-05	0.00E+00	0.00E+00	1.13E+03	1.47E+03
1-methyl-4-isopropylbenzene	134.218	0.00015	0	13.5	0	7.236E-06	0.00E+00	0.00E+00	6.30E+02	8.19E+02
1,3-diethylbenzene	134.218	0.00012	0	13.5	0	5.789E-06	0.00E+00	0.00E+00	5.04E+02	6.55E+02
1-methyl-3-propylbenzene	134.218	0.00056	0	13.5	0	2.641E-05	0.00E+00	0.00E+00	2.30E+03	2.99E+03
1-methyl-4-propylbenzene	134.218	0.00023	0	13.5	0	1.085E-05	0.00E+00	0.00E+00	9.45E+02	1.23E+03
n-butylbenzene	134.218	0.00022	0	13.5	0	1.013E-05	0.00E+00	0.00E+00	8.82E+02	1.15E+03
1,2-dimethyl-4-ethylbenzene	134.218	0.00041	0	13.5	0	1.918E-05	0.00E+00	0.00E+00	1.67E+03	2.17E+03
1-methyl-2-propylbenzene	134.218	0.00030	0	13.5	0	1.411E-05	0.00E+00	0.00E+00	1.23E+03	1.60E+03
1,4-dimethyl-2-ethylbenzene	134.218	0.00028	0	13.5	0	1.303E-05	0.00E+00	0.00E+00	1.13E+03	1.47E+03
n-C_{11}	156.308	0.00815	0	17.0	0	4.147E-04	0.00E+00	0.00E+00	3.34E+04	4.34E+04
1,3-dimethyl-4-ethylbenzene	134.218	0.00029	0	13.5	0	1.375E-05	0.00E+00	0.00E+00	1.20E+03	1.56E+03
1,3-dimethyl-5-ethylbenzene	134.218	0.00038	0	13.5	0	1.809E-05	0.00E+00	0.00E+00	1.57E+03	2.05E+03
naphthalene	128.171	0.00082	0	12.0	0	3.604E-05	0.00E+00	0.00E+00	3.37E+03	4.38E+03
C_1-naphthalenes	142.197	0.00178	0	13.5	0	7.923E-05	0.00E+00	0.00E+00	7.30E+03	9.50E+03
C_2-naphthalenes	156.224	0.00218	0	15.0	0	9.774E-05	0.00E+00	0.00E+00	8.91E+03	1.16E+04
C_3-naphthalenes	170.250	0.00162	0	16.5	0	7.356E-05	0.00E+00	0.00E+00	6.64E+03	8.64E+03
C_4-naphthalenes	184.277	0.00070	0	18.0	0	3.197E-05	0.00E+00	0.00E+00	2.87E+03	3.72E+03
1,2,3,4-tetramethylbenzene	134.218	0.00033	0	13.5	0	1.556E-05	0.00E+00	0.00E+00	1.35E+03	1.76E+03
n-C_{12}	170.335	0.00722	0	18.5	0	3.669E-04	0.00E+00	0.00E+00	2.96E+04	3.84E+04
i-C_{13}	184.361	0.00178	0	20.0	0	9.014E-05	0.00E+00	0.00E+00	7.27E+03	9.46E+03
i-C_{14}	198.388	0.00130	0	21.5	0	6.588E-05	0.00E+00	0.00E+00	5.32E+03	6.92E+03
n-C_{13}	184.361	0.00638	0	20.0	0	3.239E-04	0.00E+00	0.00E+00	2.61E+04	3.40E+04
i-C_{15}	212.415	0.00130	0	23.0	0	6.582E-05	0.00E+00	0.00E+00	5.32E+03	6.92E+03

n-C_{14}	198.388	0.00584	0	21.5	0	2.959E-04	0.00E+00	0.00E+00	2.39E+04	3.11E+04
i-C_{16}	226.441	0.00221	0	24.5	0	1.117E-04	0.00E+00	0.00E+00	9.04E+03	1.17E+04
n-C_{15}	212.415	0.00559	0	23.0	0	2.832E-04	0.00E+00	0.00E+00	2.29E+04	2.98E+04
fluorene	166.219	0.00013	0	15.5	0	5.702E-06	0.00E+00	0.00E+00	5.35E+02	6.96E+02
C_1-fluorenes	180.245	0.00034	0	17.0	0	1.493E-05	0.00E+00	0.00E+00	1.39E+03	1.80E+03
C_2-fluorenes	194.272	0.00050	0	18.5	0	2.227E-05	0.00E+00	0.00E+00	2.05E+03	2.66E+03
C_3-fluorenes	208.298	0.00045	0	20.0	0	2.003E-05	0.00E+00	0.00E+00	1.83E+03	2.37E+03
n-C_{16}	226.441	0.00467	0	24.5	0	2.366E-04	0.00E+00	0.00E+00	1.91E+04	2.49E+04
i-C_{18}	254.494	0.00149	0	27.5	0	7.541E-05	0.00E+00	0.00E+00	6.11E+03	7.94E+03
n-C_{17}	240.468	0.00411	0	26.0	0	2.081E-04	0.00E+00	0.00E+00	1.68E+04	2.19E+04
pristane	268.521	0.00241	0	29.0	0	1.216E-04	0.00E+00	0.00E+00	9.86E+03	1.28E+04
dibenzothiophene	184.258	0.00008	0	14.0	0	2.733E-06	0.00E+00	0.00E+00	3.15E+02	4.09E+02
C_1-dibenzothiophenes	198.285	0.00026	0	15.5	0	9.560E-06	0.00E+00	0.00E+00	1.07E+03	1.39E+03
C_2-dibenzothiophenes	212.311	0.00037	0	17.0	0	1.383E-05	0.00E+00	0.00E+00	1.51E+03	1.96E+03
C_3-dibenzothiophenes	226.338	0.00030	0	18.5	0	1.138E-05	0.00E+00	0.00E+00	1.22E+03	1.58E+03
C_4-dibenzothiophenes	240.364	0.00018	0	20.0	0	7.183E-06	0.00E+00	0.00E+00	7.56E+02	9.82E+02
phenanthrene	178.229	0.00031	0	16.5	0	1.332E-05	0.00E+00	0.00E+00	1.26E+03	1.64E+03
C_1-phenanthrenes	192.256	0.00076	0	18.0	0	3.334E-05	0.00E+00	0.00E+00	3.12E+03	4.05E+03
C_2-phenanthrenes	206.282	0.00083	0	19.5	0	3.672E-05	0.00E+00	0.00E+00	3.40E+03	4.42E+03
C_3-phenanthrenes	220.309	0.00058	0	21.0	0	2.589E-05	0.00E+00	0.00E+00	2.38E+03	3.09E+03
C_4-phenanthrenes	234.336	0.00028	0	22.5	0	1.243E-05	0.00E+00	0.00E+00	1.13E+03	1.47E+03
n-C_{18}	254.494	0.00335	0	27.5	0	1.695E-04	0.00E+00	0.00E+00	1.37E+04	1.78E+04
phytane	282.547	0.00144	0	30.5	0	7.261E-05	0.00E+00	0.00E+00	5.89E+03	7.65E+03
n-C_{19}	268.521	0.00297	0	29.0	0	1.500E-04	0.00E+00	0.00E+00	1.22E+04	1.58E+04
n-C_{20}	282.547	0.00259	0	30.5	0	1.309E-04	0.00E+00	0.00E+00	1.06E+04	1.38E+04
fluoranthene	202.251	0.00000	0	18.5	0	1.974E-07	0.00E+00	0.00E+00	1.89E+01	2.46E+01
pyrene	202.251	0.00002	0	18.5	0	6.581E-07	0.00E+00	0.00E+00	6.30E+01	8.19E+01
C_1-fluoranthenes/pyrenes	216.277	0.00012	0	20.0	0	5.322E-06	0.00E+00	0.00E+00	5.04E+02	6.55E+02
C_2-fluoranthenes/pyrenes	230.304	0.00019	0	21.5	0	8.395E-06	0.00E+00	0.00E+00	7.87E+02	1.02E+03
C_3-fluoranthenes/pyrenes	244.330	0.00021	0	23.0	0	9.143E-06	0.00E+00	0.00E+00	8.50E+02	1.11E+03
C_4-fluoranthenes/pyrenes	258.357	0.00015	0	24.5	0	6.822E-06	0.00E+00	0.00E+00	6.30E+02	8.19E+02
n-C_{21}	296.574	0.00211	0	32.0	0	1.063E-04	0.00E+00	0.00E+00	8.63E+03	1.12E+04
n-C_{22}	310.601	0.00185	0	33.5	0	9.311E-05	0.00E+00	0.00E+00	7.56E+03	9.82E+03
n-C_{23}	324.627	0.00158	0	35.0	0	7.989E-05	0.00E+00	0.00E+00	6.49E+03	8.43E+03
n-C_{24}	338.654	0.00140	0	36.5	0	7.056E-05	0.00E+00	0.00E+00	5.73E+03	7.45E+03
benz[*a*]anthracene	228.288	0.00002	0	21.0	0	6.618E-07	0.00E+00	0.00E+00	6.30E+01	8.19E+01
chrysene	228.288	0.00008	0	21.0	0	3.640E-06	0.00E+00	0.00E+00	3.46E+02	4.50E+02

C_1-benz[*a*]anthracenes/chrysenes	242.314	0.00018	0	22.5	0	8.016E-06	0.00E+00	0.00E+00	7.56E+02	9.82E+02
C_2-benz[*a*]anthracenes/chrysenes	256.341	0.00022	0	24.0	0	9.767E-06	0.00E+00	0.00E+00	9.13E+02	1.19E+03
C_3-benz[*a*]anthracenes/chrysenes	270.368	0.00015	0	25.5	0	6.446E-06	0.00E+00	0.00E+00	5.98E+02	7.78E+02
n-C_{25}	352.680	0.00115	0	38.0	0	5.814E-05	0.00E+00	0.00E+00	4.72E+03	6.14E+03
n-C_{26}	366.707	0.00102	0	39.5	0	5.153E-05	0.00E+00	0.00E+00	4.19E+03	5.44E+03
n-C_{27}	380.734	0.00085	0	41.0	0	4.300E-05	0.00E+00	0.00E+00	3.49E+03	4.54E+03
n-C_{28}	394.760	0.00064	0	42.5	0	3.214E-05	0.00E+00	0.00E+00	2.61E+03	3.40E+03
n-C_{29}	408.787	0.00059	0	44.0	0	2.981E-05	0.00E+00	0.00E+00	2.42E+03	3.15E+03
n-C_{30}	422.813	0.00051	0	45.5	0	2.555E-05	0.00E+00	0.00E+00	2.08E+03	2.70E+03
n-C_{31}	436.840	0.00053	0	47.0	0	2.670E-05	0.00E+00	0.00E+00	2.17E+03	2.82E+03
n-C_{32}	450.866	0.00043	0	48.5	0	2.167E-05	0.00E+00	0.00E+00	1.76E+03	2.29E+03
n-C_{33}	464.893	0.00036	0	50.0	0	1.818E-05	0.00E+00	0.00E+00	1.48E+03	1.92E+03
n-C_{34}	478.920	0.00027	0	51.5	0	1.354E-05	0.00E+00	0.00E+00	1.10E+03	1.43E+03
n-C_{35}	492.946	0.00021	0	53.0	0	1.044E-05	0.00E+00	0.00E+00	8.50E+02	1.11E+03
n-C_{36}	506.973	0.00018	0	54.5	0	8.894E-06	0.00E+00	0.00E+00	7.24E+02	9.41E+02
n-C_{37}	520.999	0.00015	0	56.0	0	7.346E-06	0.00E+00	0.00E+00	5.98E+02	7.78E+02
n-C_{38}	535.026	0.00013	0	57.5	0	6.572E-06	0.00E+00	0.00E+00	5.35E+02	6.96E+02
n-C_{39}	549.053	0.00011	0	59.0	0	5.412E-06	0.00E+00	0.00E+00	4.41E+02	5.73E+02
n-C_{40}	563.079	0.00010	0	60.5	0	5.024E-06	0.00E+00	0.00E+00	4.09E+02	5.32E+02
n-C_{41}	577.106	0.00008	0	62.0	0	3.864E-06	0.00E+00	0.00E+00	3.15E+02	4.09E+02
n-C_{42}	591.132	0.00010	0	63.5	0	5.023E-06	0.00E+00	0.00E+00	4.09E+02	5.32E+02
	Totals	0.48017			0.02965	0.01164	2.18E+06	2.83E+06	9.48E+05	1.23E+06

Oxygen removing potential of ALL Plume HC's (mol O_2/g_T)[h]	0.0413			
	Low Estimate	*High Estimate*	*average*	*plus-minus*
Total DO Anomaly (mol)[i]	3.000E+10	3.900E+10	3.450E+10	4.500E+09
Total environmental release (kg)[j]	7.265E+08	9.445E+08	8.355E+08	1.090E+08
Total environmental release rate (kg/day)[k]	8.753E+06	1.138E+07	**1.007E+07**	**1.313E+06**
Total soluble HC mass flow rate into deep plume (kg/day)[l]	2.177E+06	2.830E+06	2.503E+06	3.265E+05
Total insoluble HC mass flow rate into deep plume (kg/day)[m]	9.480E+05	1.232E+06	1.090E+06	1.422E+05

	average	plus-minus
total deep plume mass	3.594E+06	3.562E+05

a Dissolved fraction set to zero for hydrocarbons less soluble than n-C_6

b Stoichiometric ratio of O_2:hydrocarbon normalized to hydrocarbon = 1

c Oxygen removing potential of **insoluble** hydrocarbon mass
0.15 = fraction trapped relative to toluene
0.9610 = fraction of toluene dissolved
$F_x = (\sum M_i - \sum(F_i * M_i))/(1-\sum(F_i * M_i))$ is the fraction of insoluble species characterized in the MW-1 sample
$\sum M_i$ = Sum of the mass fractions characterized in the MW-1 sample = 0.480169

d Mass of dissolved hydrocarbons - Low (g) = Fi x Mi x TFl
TFl = Total HC Mass Flow Rate - Low Estimate (kg/day)

e Mass of dissolved hydrocarbons - High (g) = Fi x Mi x TFh
TFh = Total HC Mass Flow Rate - High Estimate (kg/day)

f Mass of trapped hydrocarbons - Low (g) = ((1-Fi) x Mi x 0.15 x 0.9610 x TFl) / Fx
0.15 = fraction trapped relative to toluene
0.9610 = fraction of toluene dissolved

g Mass of trapped hydrocarbons - High (g) = ((1-Fi) x Mi x 0.15 x 0.9610 x TFh) / Fx
0.15 = fraction trapped relative to toluene
0.9610 = fraction of toluene dissolved

h sum of DO removing potential of soluble + insoluble HCs

i Kessler et al., (2011) Science, 331, 312-315.

j total DO anomaly / total DO removing potential *1000

k total environmental hydrocarbon mass released divided by 83 days of spill

l Σ[Fi * Mi * total release rate into deep plume]

m Σ[((1-Fi) * Mi * 0.15 * 0.9610 * total release rate into deep plume / Fx]